• Volume 9C, Number 4, May 1961

מוסד ויצמן למדעים במדעי הטבע ובטכנולוגיה בישראל • ירושלים
The Weizmann Science Press of Israel • Jerusalem

BULLETIN OF THE RESEARCH COUNCIL OF ISRAEL

Section C TECHNOLOGY

Bull. Res. Counc. of Israel. C. Techn.
Incorporating the Scientific Publications of the Technion—Israel Institute of Technology, Haifa

The appended figure (Figure 1) belongs to the article by H. C. MANNHEIM *et al* on. page 123 of Volume 9, No. 3. The figure was inadvertently omitted from the latter issue.

FLAVOUR RECOVERY FROM ALICANT AND MUSCAT GRAPE JUICE

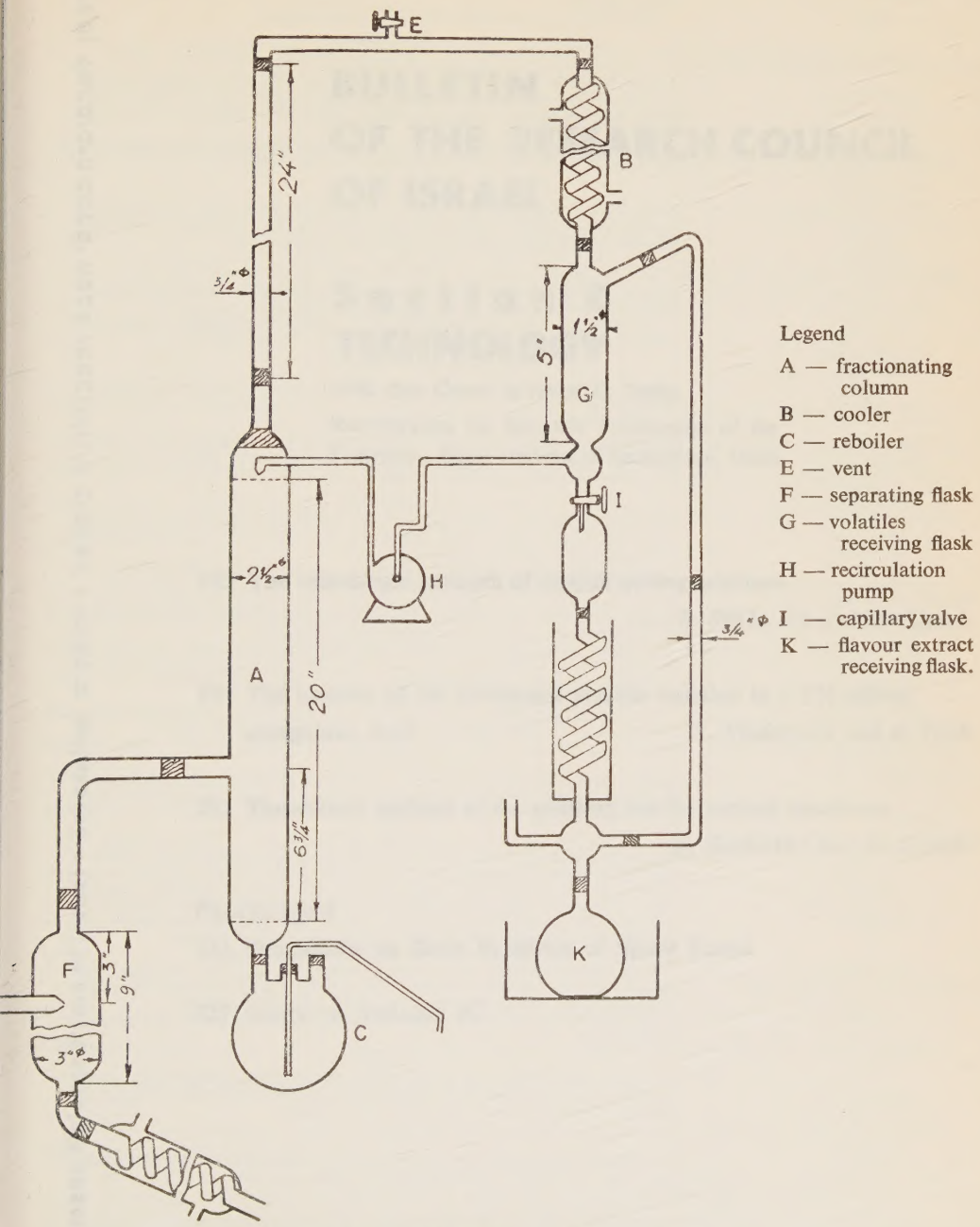

Figure 1

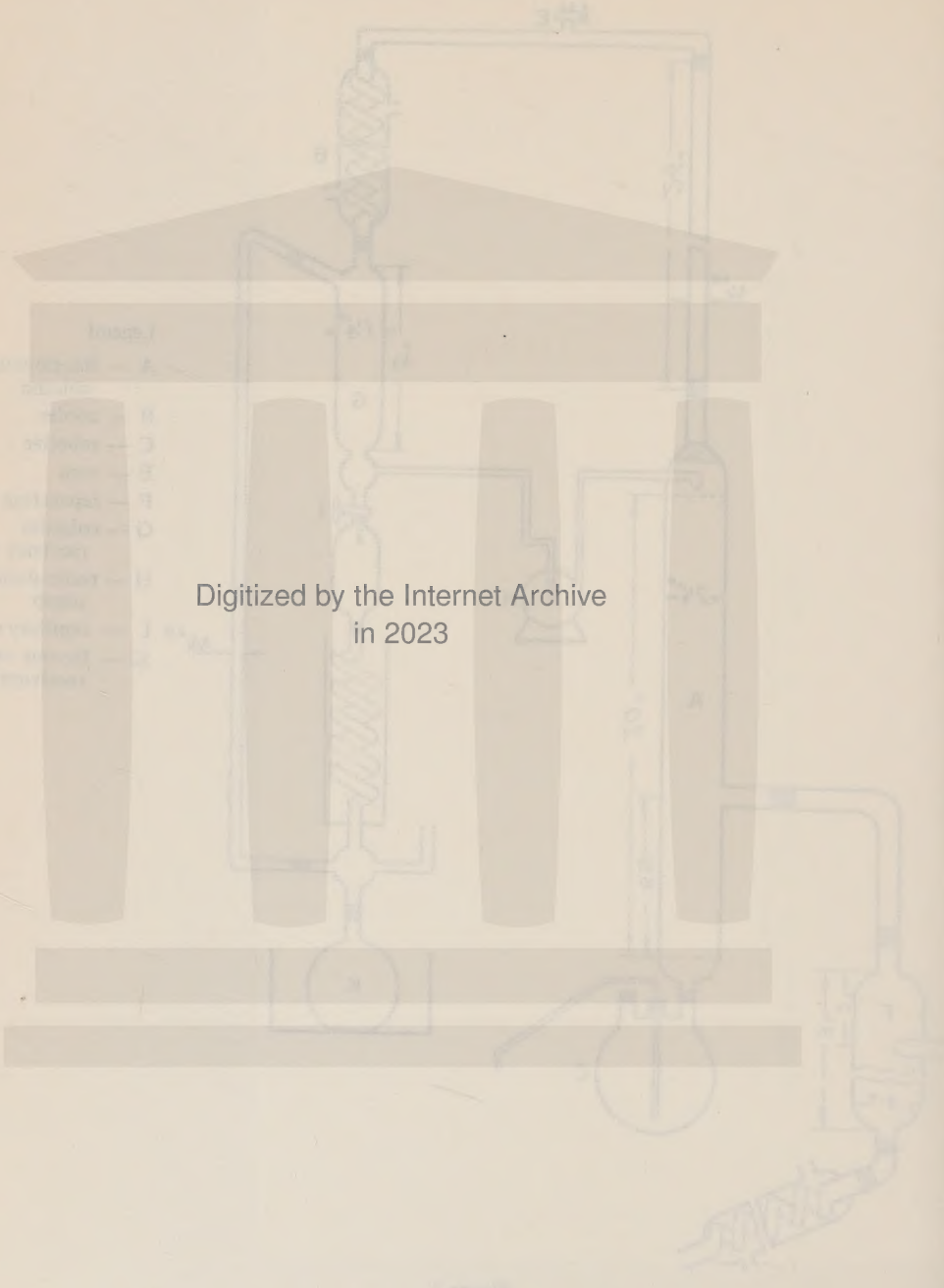

• Volume 9C, Number 4, May 1961

מוסד ויצמן למדעים במדעי הטבע ובטכנולוגיה בישראל • ירושלים

BULLETIN OF THE RESEARCH COUNCIL OF ISRAEL

Section C TECHNOLOGY

Bull. Res. Counc. of Israel. C. Techn.

Incorporating the Scientific Publications of the Technion — Israel Institute of Technology, Haifa

The Weizmann Science Press of Israel • Jerusalem

BULLETIN
OF THE RESEARCH COUNCIL
OF ISRAEL.

MIRIAM BALABAN
Editor

NOTICE TO CONTRIBUTORS

Contributors to the *Bulletin of the Research Council of Israel* should conform to the following recommendations of the editors of this journal in preparing manuscripts for the press.

Contributions must be original and should not have been published previously. When a paper has been accepted for publication, the author(s) may not publish it elsewhere unless permission is received from the Editor of this journal.

Papers may be submitted in English and in French.

MANUSCRIPT

General

Papers should be written as concisely as possible. MSS should be typewritten on one side only and double-spaced, with side margins not less than 2.5 cm wide. Pages, including those containing illustrations, references or tables, should be numbered.

The Editor reserves the right to return a MS to the author for retyping or any alterations. Authors should retain copies of their MS.

Spelling

Spelling should be based on the Oxford Dictionary and should be consistent throughout the paper. Geographic and proper names in particular should be checked for approved forms of spelling or transliteration.

Indications

Greek letters should be indicated in a legend preceding the MS, as well as by a pencil note in the margin on first appearance in the text.

When there is any room for confusion of symbols, they should be carefully differentiated, e.g. the letter "l" and the figure "1"; "O" and "0".

Abbreviations

Titles of journals should be abbreviated according to the *World List of Scientific Periodicals*.

Abstract

Every paper must be accompanied by a brief but comprehensive abstract. Although the length of the abstract is left to the discretion of the author, 3% of the total length of the paper is suggested.

References

In Sections A and C, and in Letters to the Editor in all Sections, references are to be cited in the text by number, e.g. ... Taylor' ..., and are to be arranged in the order of appearance.

In Sections B, D, E, and G, the references are to be cited in the text by the author's name and date of publication in parentheses, e.g. ... (Taylor 1932)... if the author's name is already mentioned in the text, then the year only appears in the parentheses, e.g. ... found by Taylor (1932)... The references in these Sections are to be arranged in alphabetical order.

In Section F, references are to be cited in the text by number in square brackets, e.g. ... Taylor[3].., and are to be arranged in alphabetical order.

The following form should be used:

3. TAYLOR, G.I., 1932, *Proc. roy. Soc.*, A138, 41.

Book references should be prepared according to the following form:

4. JACKSON, F., 1930, *Thermodynamics*, 4th ed., Wiley, New York.

TYPOGRAPHY

In all matters of typography the form adopted in this issue should be followed. Particular attention should be given to position of symbols, headings, etc. and type specification.

ILLUSTRATIONS

Illustrations should be sent in a state suitable for direct photographic reproduction. Line drawings should be drawn in large scale with India ink on white drawing paper, bristol board, tracing paper, blue linen, or blue-lined grahp paper. If the lettering cannot be drawn neatly by the author, he should indicate it in pencil for the guidance of the draftsman. Possible photographic reduction should be carefully considered when lettering and in other details.

Half-tone photographs should be on glossy contrast paper.

Illustrations should be mounted on separate sheets of paper on which the caption and figure number is typed. Each drawing and photograph should be identified on the back with the author's name and figure number.

The place in which the figure is to appear should be indicated on the margin of the MS.

PROOFS

Authors making revisions in proofs will be required to bear the costs thereof. Proofs should be returned to the Editor within 24 hours, otherwise no responsibility is assumed for the corrections of the author.

REPRINTS

Reprints may be ordered at the time the proof is returned. A table designating the cost of reprints may be obtained on request.

Orders in America should be addressed to the Weizmann Science Press, P.O.B. 801 Jerusalem or through booksellers, and in England and Europe to Wm. Dawson and Sons, Ltd. Cannon House, Macklin Street, London W.C. 2, directly or through booksellers. Annual subscription per section (four issues): IL. 6.000 ($6.00, £2.02). Single copy: IL. 1.500 $1.50. 12s.) — Manuscripts should be addressed: The Editor. The Weizmann Science Press of Israel, P.O.B. 801 Jerusalem, 33 King George Ave. Telephone 27844, 26345.

THE ANISOTROPIC STRENGTH OF ASPHALT PAVING MIXTURES

E. SHKLARSKY AND M. LIVNEH*

Highway and Soil Engineering Laboratory, Technion-Israel Institute of Technology, Haifa

ABSTRACT

A laboratory study of compacted asphalt paving mixtures has shown that their strength is not isotropic. Preliminary test results are reported and discussed, and a modification of the bearing capacity formula is proposed.

INTRODUCTION

The bearing capacity of a compacted asphalt mixture depends primarily on its strength characteristics. Hitherto, bearing capacity predictions have been based on the assumption that this strength is isotropic, i.e. independent of orientation. This assumption, however, was not borne out in a laboratory study carried out by the authors.

PRELIMINARY TEST RESULTS

Two types of mixtures were prepared, one made with crushed limestone aggregate and the other with clean dune sand (see Figure 1). The bitumen used for both series was 80/100 penetration. The samples were compacted in 12 cm cubical moulds at an effort (energy per unit volume) equivalent to that of the Marshall method. Each type was studied by means of a simple compression test** in two series, with the load applied parallel and perpendicular to the direction of compaction respectively. The test results are plotted in Figure 2, and clearly show that a definite ratio m', greater than 1, exists between the two respective strength values σ_{par} and σ_{perp}:

$$m' = \frac{\sigma_{par}}{\sigma_{perp}} > 1 \qquad (1)$$

The ratio was also found to increase with the density of the compacted asphalt up to a maximum value, after which it decreases with increasing density towards its asymptotic value of 1 (see Figure 3). It is believed that for the uncompacted asphalt the ratio equals 1.

---

* The paper is based on the second author's research work towards the D.Sc. degree under the supervision of the first author.

** The asphalt concrete cubes were tested according to the Marshall procedure, i.e. after soaking in hot water (60°C) for half an hour; the sand-asphalt cubes were tested without preliminary soaking. The rate of compression was also according to the Marshall method, i.e. 2 inch/min.

Received November 18, 1960.

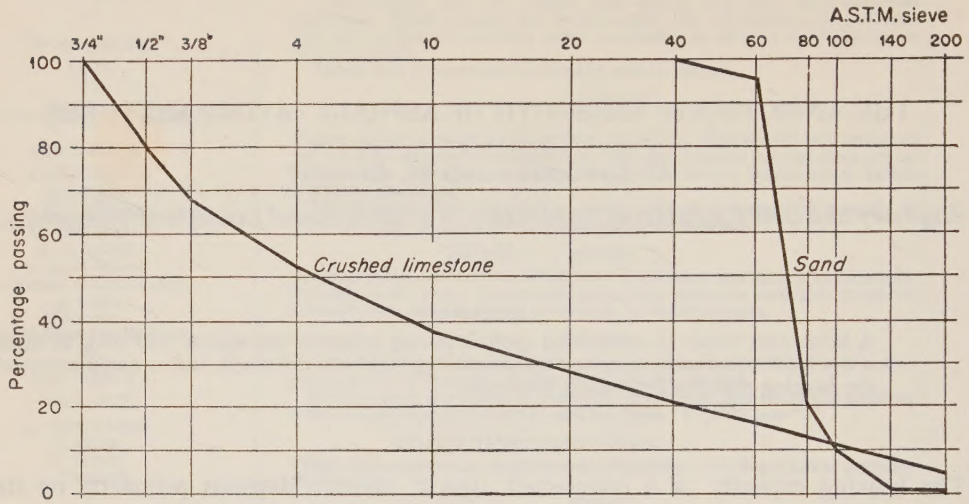

Figure 1
Aggregate grading for bituminous concrete and sand-asphalt mixtures

DISCUSSION

The theory put forward by Casagrande and Carillo[1] on anisotropic materials is extended here to include materials possessing both components of shear resistance, i.e. variable cohesion and constant internal friction.

It is assumed that the compacted asphalt is anisotropic and has three strength parameters, namely φ_e — the constant angle of internal friction of the material for any given plane; C_{par} — the cohesion coefficient parallel to the direction of compaction; and C_{perp} — the cohesion coefficient perpendicular to the direction of compaction. The value of the cohesion in a plane at an angle α with the principal horizontal plane (which is in turn at right angles to the direction of compaction) is, according to the above theory,

$$C_\alpha = C_{perp} + (C_{par} - C_{perp}) \sin^2\alpha \tag{2}$$

If a compacted sample is subjected to the principal stresses σ_{perp} (minor) and σ_{par} (major), the shear strength S under triaxial test conditions will be:

$$S = C_{perp} + (C_{par} - C_{perp})\sin^2\alpha_0 + \sigma_n \tan\varphi_e \tag{3}$$

where α_0 is the angle of inclination of the critical plane, and σ_n the stress normal to it.

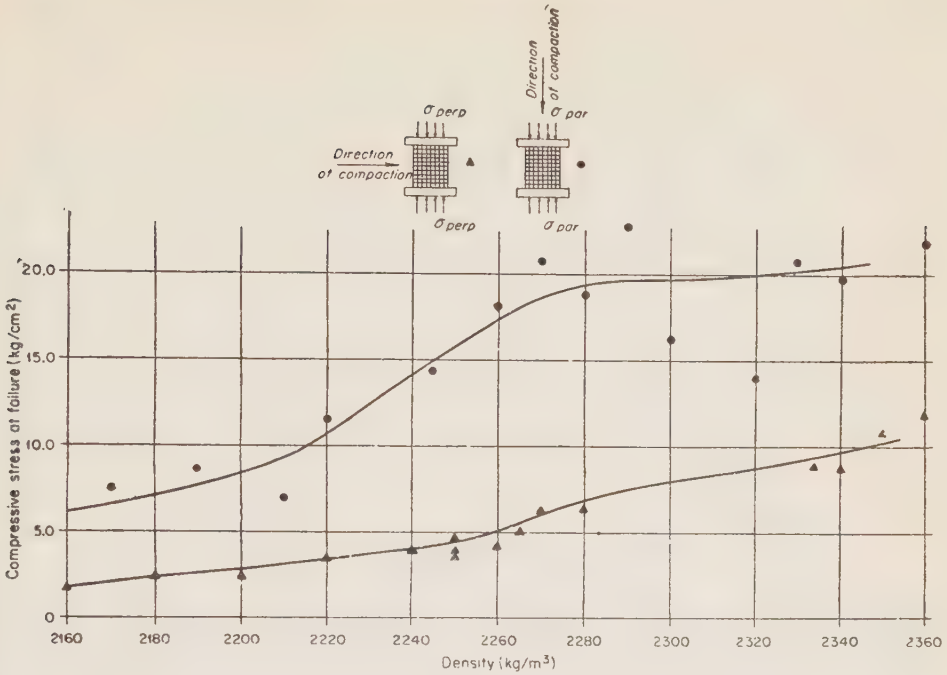

Figure 2a

Compressive stress at failure versus density (asphalt concrete cubes)

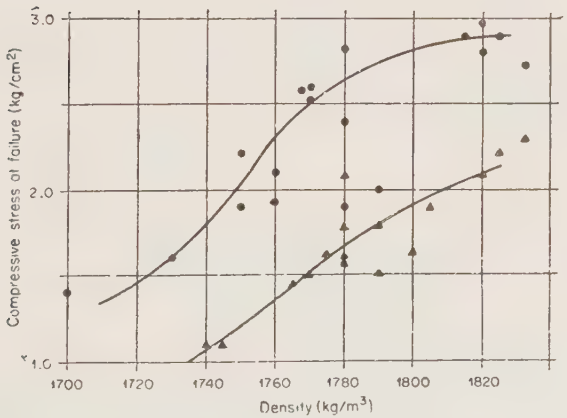

Figure 2b

Compressive stress at failure versus density (sand-asphalt cubes)

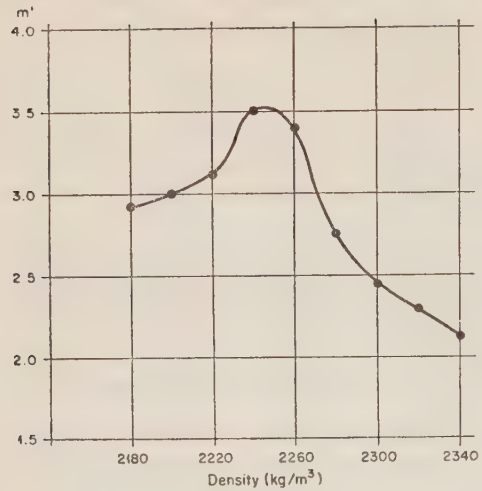

Figure 3a
Asphalt concrete cubes

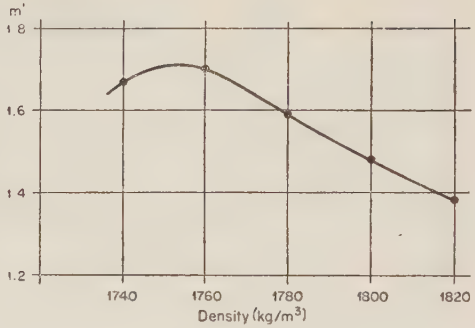

Figure 3b
Sand-asphalt cubes

m' versus density (points computed from Figure 2b)

According to Mohr's theory of rupture, the strength line given by eq. (3) is tangent to the critical stress circle. Hence (see App. I) the radius R of the latter is

$$R = (C_{par} + \sigma_{perp}\tan\varphi_e)\tan\varphi_e +$$

$$+ \sqrt{\tan^2\varphi_e(C_{par} + \sigma_{perp}\tan\varphi_e)^2 + (C_{par} + \sigma_{perp}\tan\varphi_e)(C_{perp} + \sigma_{perp}\tan\varphi_e)} \quad (4)^*$$

The critical value of the angle α_0 is given by

$$\tan\alpha_0 = \sqrt{\frac{C_{perp} + \sigma_{perp}\tan\varphi_e + 2R\tan\varphi_e}{C_{par} + \sigma_{perp}\tan\varphi_e}} \quad (5)$$

For $C_{perp} = C_{par}$, eq. (4) and (5) are reduced to the well-known equations of the critical stress circles for isotropic materials.

As shown in App. II, eq. (4) can be rewritten with sufficient accuracy in the following form

$$R = C_{par}\tan\varphi_e + \sqrt{C^2_{par}\tan^2\varphi_e + C_{par}C_{perp}} + \frac{\sigma_{perp}\sin\varphi_e}{1 - \sin\varphi_e} \quad (6)$$

The line S', tangent to the critical circle, is thus a straight line of the form:

$$S' = C + \sigma_n\tan\varphi \quad (7)$$

where C is given by

$$C = \left(C_{par}\tan\varphi_e + \sqrt{C^2_{par}\tan^2\varphi_e + C_{par}C_{perp}}\right)\left(\frac{1 - \sin\varphi_e}{\cos\varphi_e}\right) \quad (8)$$

* This expression can also be obtained by substituting $\varphi_1 = \varphi_3 = \varphi_e$ = const. in eq. (7) in Hank and McCarthy's paper[2].

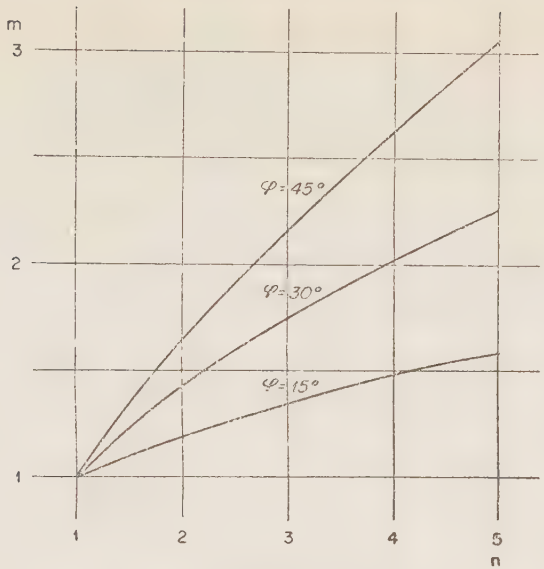

Figure 4
m versus n for $\varphi = 15°, 30°, 45°$

S' is in fact the strength line obtained in the triaxial compression test, C being the apparent cohesion and φ the angle of internal resistance. It is thus seen that C is dependent on C_{perp}, C_{par} and φ_e, and φ equals φ_e provided eq. (6) is sufficiently accurate. Eq. (8), in turn, can be rewritten in the following form:

$$C = C_{par}\left(\frac{1-\sin\varphi_e}{\cos\varphi_e}\right)\left(\tan\varphi_e + \sqrt{\tan^2\varphi_e + \frac{1}{n}}\right) \tag{9}$$

where

$$n = \frac{C_{par}}{C_{perp}} \tag{10}$$

As already stated, eq. (9) is valid if σ_{par} is the major principal stress; if it is the minor principal stress, the apparent cohesion C is replaced by C', which equals:

$$C' = \frac{C_{par}}{n}\left(\frac{1-\sin\varphi_e}{\cos\varphi_e}\right)\left(\tan\varphi_e + \sqrt{\tan^2\varphi_e + n}\right) \tag{11}$$

their ratio being

$$m = \frac{C}{C'} = \frac{n\left(\tan\varphi_e + \sqrt{\tan^2\varphi_e + \frac{1}{n}}\right)}{\tan\varphi_e + \sqrt{\tan^2\varphi_e + n}} \tag{12}$$

The ratio m is the counterpart of m' [Eq. (1)] allowing for the difference between the simple compression test carried out on the asphalt cubes and the unconfined compression test. The existence of m' also proves that of m, which is plotted against n for $\varphi_e = 15, 30, 45°$ resp. in Figure 4; the diagram explains the high values of

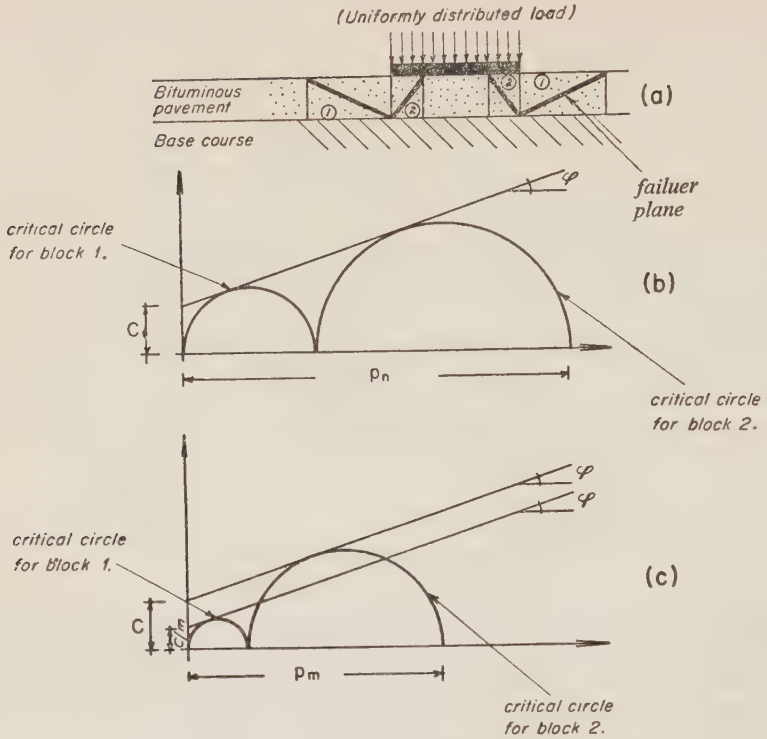

Figure 5

Bearing capacity [(a) and (b) — isotropic cohesion; (c) — anisotropic cohesion]

m' obtained for the asphalt concrete mixture compared with the low values obtained for the sand-asphalt mixture: for a given n, m' increases with increasing φ_e, and the latter is in fact higher for asphalt concrete mixtures.

MODIFICATION OF THE BEARING CAPACITY EQUATIONS

McLeod[3] suggested the following equation for the bearing capacity of asphalt paving mixtures:

$$p_n = \frac{4C}{1 - \sin\varphi}\sqrt{\frac{1 + \sin\varphi}{1 - \sin\varphi}} \tag{13}$$

where p_n is the ultimate pressure and C the apparent cohesion*. For the assumptions underlying this equation, see Figures 5a and 5b.

* As the anisotropy of the material is not taken into consideration in McLeod's equation, it is obvious that the apparent cohesion in question is the conventional value obtained in a triaxial test, with σ_{par} the major principal stress.

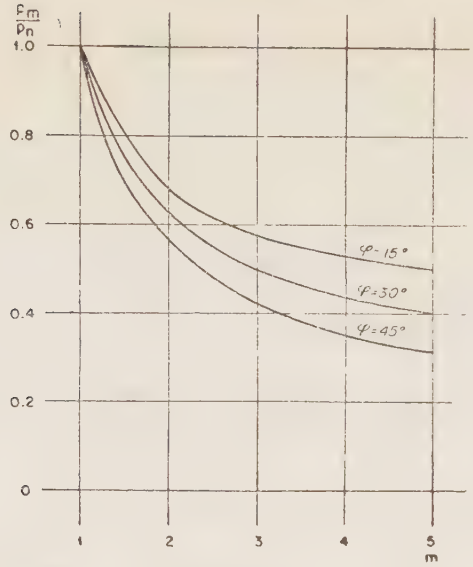

Figure 6
p_m/p_n versus m for $\varphi = 15°, 30°, 45°$

However, taking the anisotropic cohesion into consideration, eq. (13) becomes (see Figure 5c):

$$p_m = \frac{4C}{1-\sin\varphi}\sqrt{\frac{1+\sin\varphi}{1-\sin\varphi}} \times \tfrac{1}{2}\left(\frac{1+\sin\varphi}{m} + 1 - \sin\varphi\right) \tag{14}$$

or

$$p_m = p_n \times \tfrac{1}{2}\left(\frac{1+\sin\varphi}{m} + 1 - \sin\varphi\right) \tag{15}$$

The ratio $\frac{p_m}{p_n}$ is plotted against m in Figure 6. For $m = 5$ and $\varphi = 30°$, $\frac{p_m}{p_n} = 0.4$. This result is of importance, since due to the anisotrop c cohesion the safety factoe for the allowable bearing pressure is considerably lower acording to eq. (13). Boths eq. (15) and eq. (13) have to be modified further to allow for factors not taken into account. In fact, eq. (15) is only an attempt to show the importance of considering the anisotropic strengths in the case of asphalt paving mixtutes.

APPENDIX I

According to Mohr's theory, rupture occurs when the difference between strength (S) and shearing stress (τ) is a minimum and zero. Under triaxial test conditions with a given radius R of the stress circle, S and τ are functions of α, the angle of inclination of the plane under consideration. The rupture conditions are thus

$$\frac{dS}{d\alpha} - \frac{d\tau}{d\alpha} = 0 \tag{a}$$

and

$$S - \tau = 0 \tag{b}$$

Bearing in mind that $\tau = R \sin 2\alpha$, eq. (a) becomes

$$\frac{dS}{d\alpha} = 2R \cos \alpha \tag{c}$$

and eq. (b):

$$S = R \sin 2\alpha \tag{d}$$

Substituting R from eq. (d) in eq. (c), we obtain:

$$\frac{dS}{d\alpha} = 2R \cos 2\alpha = \frac{2S \cos \alpha}{\sin 2\alpha} = \frac{2S}{\tan 2\alpha} \tag{e}$$

and substituting S from eq. (3), eq. (e) becomes

$$2 \cot \varphi_e \left[C_{\text{perp}} + \sigma_{\text{perp}} \tan \varphi_e + (C_{\text{par}} - C_{\text{perp}}) \sin^2 \alpha + 2R \cos^2 \alpha_o \tan \varphi_e\right] =$$

$$= (C_{\text{par}} - C_{\text{perp}}) \sin 2\alpha_0 - R \tan \varphi_e \sin 2\alpha. \tag{f}$$

Rearranging eq. (f) we obtain the critical value of the angle of inclination [eq. (5)], and finally, substituting eq. (5) in eq. (d) the radius of the critical stress circle [eq. (4)].

APPENDIX II

The expression for R (qe. 4) can be rewritten as

$$R = \left[(1 + B \tan \varphi_e) \tan \varphi_e + \sqrt{\left(D + \frac{B \tan \varphi_e}{\cos \varphi_e}\right)^2 + B\Delta}\right] C_{\text{par}} \tag{a}$$

where:

$$D = \sqrt{\tan^2 \varphi_e + \frac{1}{n}};\ B = \frac{\sigma_{\text{perp}}}{C_{\text{perp}}};\ n = \frac{C_{\text{par}}}{C_{\text{perp}}} > 1, \quad \text{and}$$

$$\Delta = \tan \varphi_e \left(1 + 2 \tan^2 \varphi_e + \tfrac{1}{2} - \frac{2}{\cos \varphi_e} \sqrt{\tan^2 \varphi_e + \frac{1}{n}}\right)$$

Neglecting the term $B\Delta$, eq. (a) becomes:

$$R' = \left[(1 + B \tan \varphi_e) \tan \varphi_e + D + \frac{B \tan \varphi_e}{\cos \varphi_e}\right] C_{\text{par}} \tag{b}$$

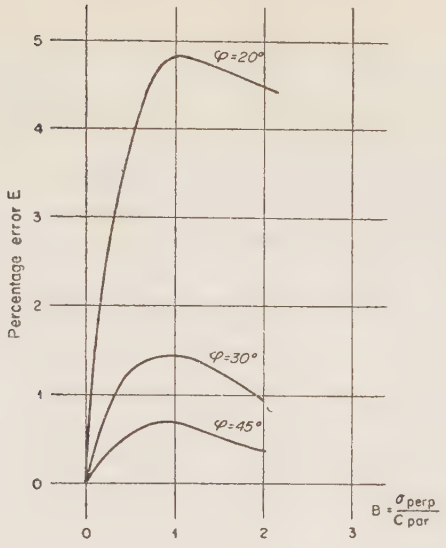

Figure 7

Percentage error E versus B for $\varphi = 20°, 30°, 45°$ at $n = 10$

which is identical with eq. (6). The percentage error E involved in omitting the term $B\Delta$ is

$$E = \frac{R - R'}{R} \times 100 = \frac{\sqrt{\left(D + \frac{B \tan \varphi_e}{\cos \varphi_e}\right)^2 + B\Delta} - \left(D + \frac{B \tan \varphi_e}{\cos \varphi_e}\right)}{(1 + B \tan \varphi_e) \tan \varphi_e + \sqrt{\left(D + \frac{B \tan \varphi_e}{\cos \varphi_e}\right)^2 + B\Delta}} \times 100 \quad \text{(c)}$$

showing that E increases with n.

E is plotted against B in Figure 7, for $n = 10$ (a reasonably high value) and practical values of φ_e. The diagram shows that the maximum possible error under these circumstances is about 5% for $\varphi_e = 20°$ and about 1.5% for $\varphi_e = 30°$. According to Nijboer[4], the accuracy of the triaxial compression test is 30% for φ and 10% for C. Substituting these values in eq. (a) we obtain

$$\frac{1}{E'} = 0.1(1 + B \tan \varphi_e) \quad \text{(d)}$$

where E' is the percentage error involved in predicting R in the triaxial compression test for isotropic materials; comparing it with the error plotted in Figure 7, it can be conclusively stated that the accuracy of eq. (b) is sufficient.

REFERENCES

1. CASAGRANDE, A. AND CARILLO, N., 1944, Shear failure of anisotropic materials, *Journal of the Boston Society of Civil Engineers*, **31,4,** 122–135.

2. HANK, R. J. AND MCCARTHY, L. E., 1948, Shear failure in anisotropic materials possessing any values of cohesion and angle of internal friction, Highway Research Board, *Proceedings, Twenty-Eighth Annual Meeting*, Washington, D.C.

3. GOETZ, W. H., 1952, Comparison of triaxial and Marshall test results (incl. discussion by N. W. McLeod). *Engineering Reprint* 72, Purdue Engineering Experimental Station.

4. NIJBOER, L. W., 1948, *Plasticity as a factor in the design of dense bituminous road carpets*, Elsevier, Amsterdam.

THE KINETICS OF THE ISOTHERMAL PEARLITE REACTION IN A 2% SILICON-MANGANESE STEEL

S. Niedzwiedz and A. Taub*

Israel Institute of Metals, Technion–Israel Institute of Technology, Haifa

ABSTRACT

The transformation characteristics of a silicon steel were investigated in the pearlitic zone. The main object of the study was identification of the relevant area in the time-temperature transformation diagram and determination of the isothermal reaction. The activation energy of the process was calculated.

The morphology and mechanical properties of the pearlites formed at different temperatures were also observed.

The pearlitic reaction of a high-silicon steel of the composition: C–0.63%, Mn–0.99%, Si–1.88%, Cr–0.41%, S–0.006%, P–0.037%, was studied. The beginning and end of the transformation were determined under isothermal conditions for different temperatures, whereby the pearlitic zone of the time-temperature transformation (TTT) diagram of this steel was identified. The transformed fractions were measured as a function of time under the microscope and the results used in the analysis of the kinetics of the reaction. The morphology and mechanical properties of the decomposed product were also observed.

The procedure employed is described schematically in Figure 1. Small specimens are austenitised (step a) and subsequently transferred (step b) to a constant-temperature bath of liquid metal at temperature t_p (between the A_1 and "knee" temperatures) at which they are kept for progressively increasing periods of time, resulting in increasing amounts of pearlite in a decreasing amount of austenitic matrix at the given temperature. After the corresponding period, each group of three specimens is transferred very rapidly (step d) to a water quenching bath at room temperature, where the remaining austenite is transformed into martensite. The specimens thus contain both pearlite and untempered martensite, differentiated under the microscope through the selective action of the etching medium (nital or picral) which reveals them as dark- and light-etch areas respectively.

In the present experiments, specimens 8 mm in diameter and 2 mm thick were heated in a molten-tin bath, in three parallel series, at successive temperatures from 700°C to 625°C in 25°C intervals. Each specimen was placed in the heating chamber of a furnace for five minutes[1] at the austenitising temperature (830°C)

* The Arturo Gruenebaum Chair of Mining and Metallurgy.

Received November 27, 1960

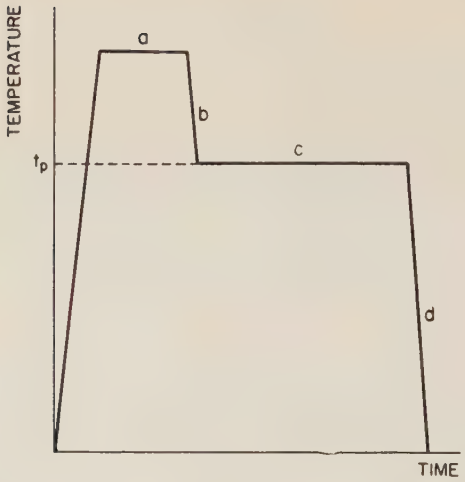

Figure 1
Schematic descripton of heat treatment

and then transferred to the bath for the predetermined period of time and finally to the water bath held at room temperature. The treated specimens were subjected to microscopic examination in which the relative proportions of light and dark areas in the microstructure (as shown in Figures 2 and 3) were determined, using

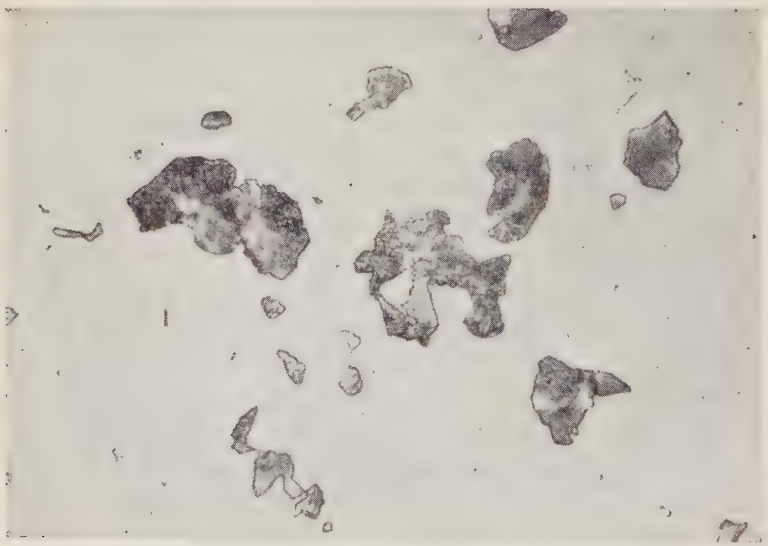

Figure 2
Magnification: ×500 Etch: Picral 4%
Specimen kept isothermally at 700°C for 40 seconds after austenitisation and subsequently quenched to room temperature. Dark areas 15% pearlite; light areas 85% martensite

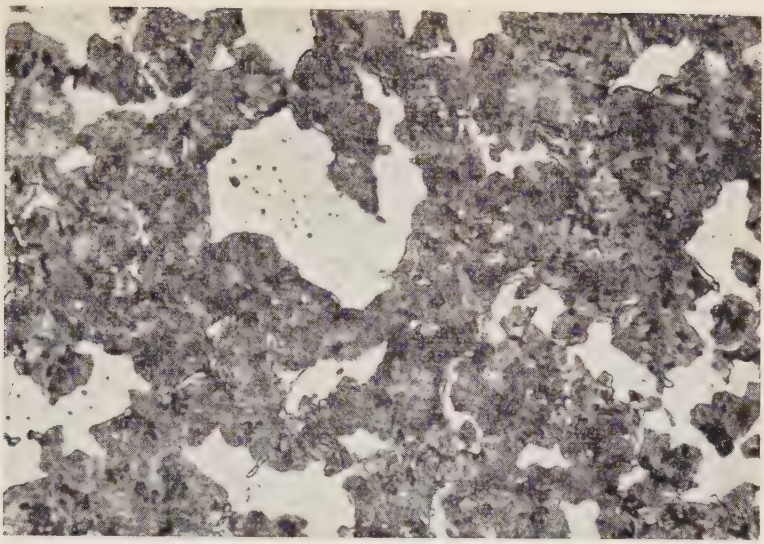

Figure 3

Magnification: ×500 Etch: Nital 2%

Specimen kept isothermally at 650°C for 25 seconds after austenitisation and subsequently quenched to room temperature. Dark areas 85% pearlite: light areas 15% martensite

the electric semi-automatic counter developed by Hulburt,[3] by Rosiwal's method of lineal analysis[2], based on the measurement of line intercepts across the different areas in a number of random directions (four in the present case, making a total of twelve measurements per series).*

The mean, standard deviation, and standard error of the mean were calculated from the readings obtained for each series. The four traverses made gave a 95% probability of the error of the mean not exceeding 1%. The average for each time-temperature combination was plotted in the diagram shown in Figure 4, giving the pearlite content (in percent) as a function of time, with temperature as a parameter. These curves are the actual reaction curves for the process.

The reaction curves of Figure 2 were used for the construction of the pearlitic zone of the TTT diagram of the steel in question, shown in Figure 5. The graphical method employed is illustrated in Figure 6. In view of the difficulty in identifying the exact beginning and end of the reaction, the 1% and 99% transformation levels respectively were used instead.

* In order to eliminate the operative error factor, the specimens were tested completely at random instead of in order of treatment.

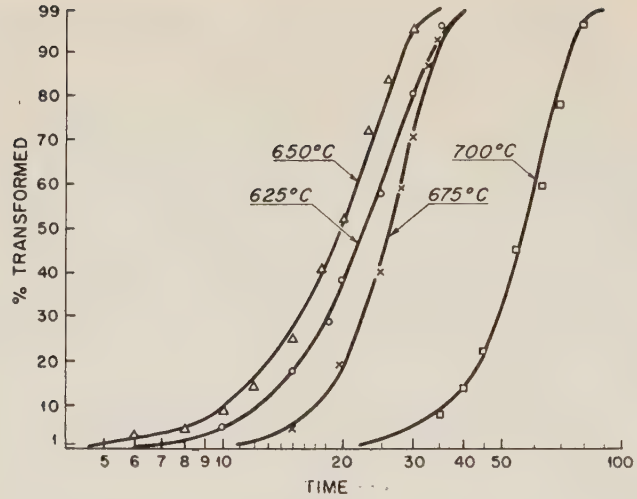

Figure 4
Experimental isothermal reaction curves, giving the pearlite content in percent as a function of time at various temperatures

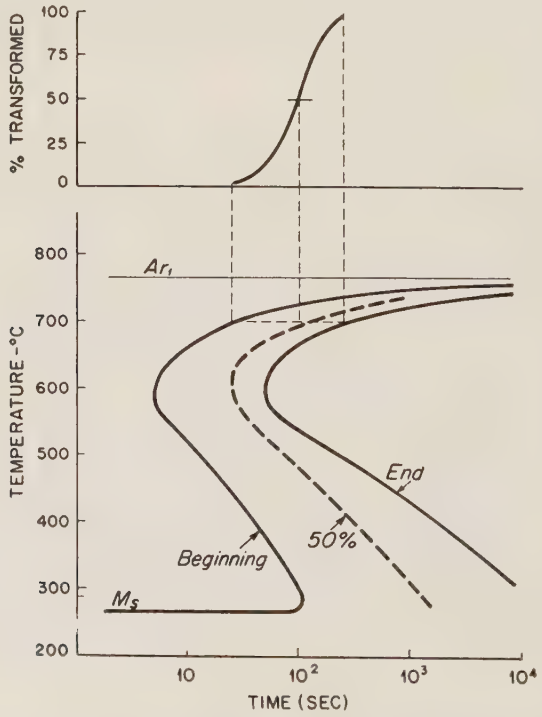

Figure 5
Method employed for construction of the TTT curve from the isothermal reaction curves

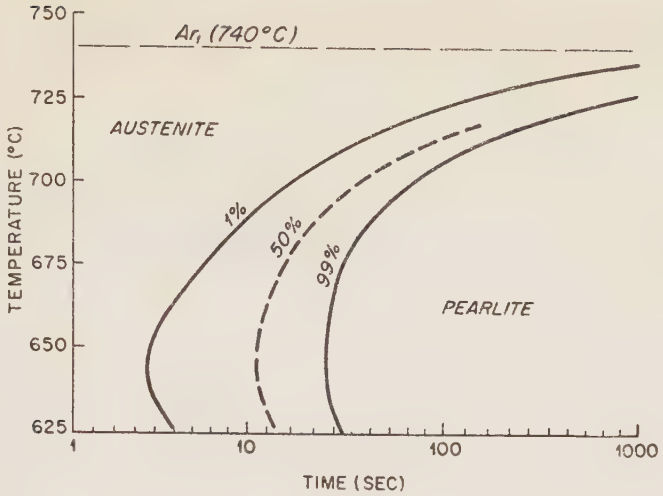

Figure 6
The pearlitic zone of the time-temperature transformation curve

The sigmoid reaction curves of Figure 4 served as a basis for the determination of the kinetics of the reaction. The curves are represented by the equation:

$$y = 1 - e^{-mt^n} \tag{1}$$

where: y — fraction of transformed austenite;
t — reaction time;
m,n — constants for a given curve.

Differentiating eq. (1) with respect to time, we obtain

$$\frac{dy}{dt} = nmt^{n-1}e^{-mt^n} \tag{2}$$

The maximum point of the derivative is the point of inflection of the sigmoid curves. Differentiating eq. (2) and equating to zero, we obtain

$$\frac{d^2y}{dt^2} = nme^{-mt^n}[-nmt^{2(n-1)} + (n-1)t^{n-2}] = 0$$

whence $nmt^n = n-1$

and

$$t = \sqrt[n]{\frac{n-1}{nm}}; \tag{3}$$

substituting in eq. (1)

$$y = 1 - e^{\frac{1-n}{n}}$$

The calculated values of n for the temperatures used in the present experiments are given in Table I below:

TABLE I.

Constants n,m for isothermal reactions

Temperature °C	n	95% confidence limit for n	$m(\times 10^{-8})$
700	4.43	±0.4	1.122
675	4.64	±0.7	17.740
650	2.92	±0.4	4372
625	3.16	±0.8	3457

The table shows that around the "knee" of the TTT curve $n=3$, for which $y=1-e^{-\frac{2}{3}}=$ $= 0.45$, while near the critical Ar_1 point $n = 4$, for which $y = 1-e^{-\frac{3}{4}} = 0.51$.

These results have a definite physical significance. Up to the point of inflection the reaction is accelerated; beyond it, it begins to decelerate due to the effect of impingement, while the point of inflection itself is characterised by an intermediate maximum rate of transformation.

It can be seen that the points of inflection of the transformation curves occur at lower fractions of the total transformation as the transformation temperature approaches that corresponding to the "knee" of the TTT curve. The constant n can thus be used as an indicator in comparing the rates of pearlitic transformation for different isothermal reactions. The variation of n is due to the formation morphology of the pearlites which is due in turn to the rates of nucleation and growth.

Eq. (2) can be used for calculating the activation energy of the process. In fact, it was shown by Zener[4] that the product nm provides for the temperature dependence of the reaction velocity, embodying as it does the rates of nucleation and growth (both of them temperature-dependent) conforming to the Boltzman distribution law,

$$nm = Ce^{-Q_a/RT} \tag{4}$$

(Q_a — activation energy, C — constant). Using eq. (1) in logarithmic form for a given value of y, we obtain

$$-\ln(1-y)=\ln\frac{1}{1-y}=mt^n=b$$

where b is constant for a given case, or $t = \sqrt[n]{\frac{b}{m}}$

Substituting m from eq. (4), we obtain

$$t = \sqrt[n]{\frac{nb}{C} e^{Q_a/RT}}$$

or

$$t = C' e^{Q_k/RT} \tag{5}$$

where Q_k is defined as Q_a/n; or, again in logarithmic form,

$$\ln t = \frac{Q_k}{RT} + \ln C' \tag{6}$$

If $\ln t$ were plotted against $1/T$, one would expect a straight line for Q_k. However, in the pearlitic zone a curve with a negative slope would be obtained, since the graph would have to resemble a TTT curve[5]. Hence in this case Q_k can only be calculated from

$$t_1 = C' e^{(Q_k + H)/RT} \tag{7}$$

where H is temperature-dependent. For the pearlitic-bainitic transition zone[6], Q_k = 72,000 cal/mol; solving eq. (7) graphically for 700°C as shown in Figure 7, we find Q_k = 77,000 cal/mol or $Q_a = nQ_k$ = 308,000 cal/mol.

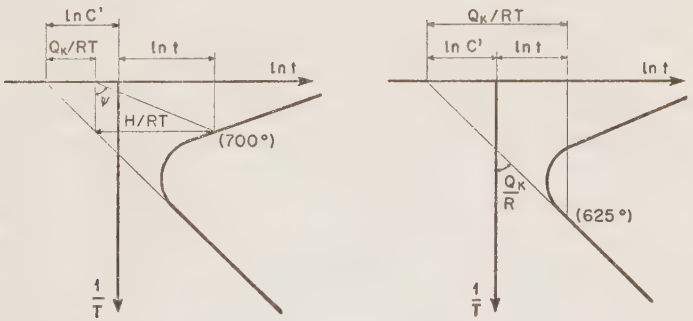

Figure 7
Graphical solution of eq. (7) for H

A peculiar feature of the steel under consideration, as observed under the microscope, is that a lamellar structure is also formed below the "knee" of the TTT curve at 625°C. This shows that the pearlite reaction reaches a maximum rate at the "knee". while lamellar structures are formed both above and below this point. Unfortunately, the methods used in the present study were not sufficiently sensitive to esta-

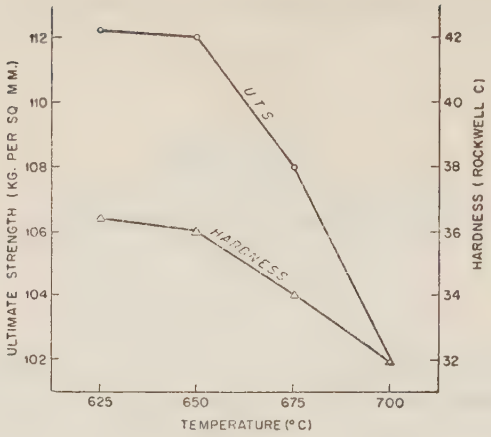

Figure 8
Mechanical properties of the pearlitic structures as a function of the transformation temperature

blish whether the rates of nucleation and growth also pass through a maximum and further research on this point would be justified.

Below 625°C a transitory structure is formed, apparently a mixture of lamellar pearlite and feathery bainite.

The steel under consideration was found to be nearly eutectoid. Only traces of hypo-eutectoid ferrite could be detected (precipitated at the former austenitic grain boundaries) and their influence could only be negligible.

Finally, the transformed specimens were studied with a view to determining the effect of variations in the inter-lamellar spacing of the pearlite upon the mechanical properties of the steel. Hardness tests were carried out on the Rockwell C scale (limit of accuracy $\pm$ 1 point) and tensile tests — on a Hounsfield tensometer, using specimens 3.57 mm in diameter and 12.6 mm in length, i.e., with an initial cross-section of 10 sq. mm and length-to-diameter ratio of 4. The average elongation for the entire pearlitic zone was found to be 15%, with a slight increase at the "knee", and the Charpy impact tests showed an average value of 0.4 kg-m. Plastic deformation prior to "necking" was relatively small, which indicates a low value for the coefficient of strain hardening. The relation between hardness, U.T.S. and transformation temperature is shown in Figure 8.

The machinability of all the pearlitic structures of the steel was found to be low (in spite of the low coefficient of strain hardening); hence it is not recommended for operations involving extensive machining.

Comparison of the hardness values reported here with those obtained on tempering martensitic structures of the same steel[7] reveals that isothermally formed pearlite is equal in hardness to the decomposition product obtained by 30 minutes' tempering at similar temperatures.

REFERENCES

1. Rosen, A. and Taub, A., 1959, An Investigation of the Martensitic Area of the Time-Temperature Transformation Diagram of a High-Silicon Carbon Steel, *Bull. Res. Counc. of Israel*, **7C**, 4.
2. Rosiwal, A., 1898. Ueber geometrische Gesteinsanalysen, Ein einfacher Weg zur ziffermässigen Feststellung der Mineralbestandteile gemengter Gesteine, *Verhandlungen der K.K. Geologischen Reichsanstalt*, **5–6**, 143.
3. Howard, R. T. and Cohen M., 1947, Qualitative Metallography by Point Counting and Lineal Analysis, *AIME Tech. Publ.*, 2215.
4. Zener, C., 1949, Theory of Growth of Spherical Precipitates, *Journal of Applied Physics*, **20**, 950.
5. Hardy, H. K. and Heal, T. J., 1956. The Mechanism of Phase Transformation in Metals (symposium), Nucleation and Growth Processes in Metals and Alloys, *The Institute of Metals*, Monograph 18, 1.
6. Rosenberg, M., 1960, Investigation of the Bainitic Zone in the TTT Diagram of a High-Silicon Steel, *Matechet*, **2**, 4. *Israel Institute of Metals, Technion – Israel Institute of Technology*. (In Hebrew).
7. Niedzwiedz, S. and Taub, A., 1960, The Tempering Characteristics of a Commercial High-Silicon, Low-Chromium Carbon Steel, *Metal Treating*, **11**, 12.

THEORETICAL ANALYSIS OF THE SPLITTING TEST FOR ASPHALT SPECIMENS

E. SHKLARSKY AND M. LIVNEH*

Highway and Soil Engineering Laboratory, Technion–Israel Institute of Technology, Haifa

ABSTRACT

The splitting test used in determining the strength of concrete specimens is applied to asphalt paving mixtures. A theory is proposed for the failure mechanism, using a stress distribution obeying Hooke's law for the elastic stage, and an anisotropic strength curve assuming a constant angle of internal friction and a variable cohesion coefficient—for the plastic stage.

Satisfactory agreement was obtained between the proposed theory and laboratory experiments. The importance of these findings lies in the possibility of utilising the theoretical equations in determining the relationships between the failure stress and the height of the specimen, as well as the anisotropic cohesion from perpendicular and parallel splitting tests.

1. INTRODUCTION

The ideal procedure for determining the strength of asphalt specimens is one which would permit laboratory design of the product on the one hand and field control on the other, using an analytical method based on strength properties governed by the quality of the product but independent of the type of test. This requirement is only partially satisfied in the testing procedures in use at present. For example, the Marshall test[1] permits both laboratory design and field control, but without any reference to the strength properties described above. Conversely, the triaxial shear test[1], although based on the angle of internal friction and cohesion, does not permit field control.**

---

* The paper is based on part on the second author's research work for the D.Sc. degree under the supervision of the first author.

** Field control of asphalt paving mixtures by the triaxial test technique is impracticable owing to the requirement limiting the height-diameter ratio of the specimen to 1.5 – 2. The thickness of the asphalt layer being about 5 cm, the corresponding diameter would be 2.5–3 cm; such a specimen would necessarily be unrepresentative considering the grain size of the asphalt($\leqq$ 2 cm), the minimum required ratio between diameter and maximum grain being 4 : 1.

Received May 9, 1961.

These circumstances have led the authors to adopt a different method constituting a far closer approach to the ideal testing procedure. The splitting test*, also known as the "Brazilian test" and commonly used in determining the tensile strength of concrete, consists in applying a load by means of two parallel sticks to a concrete cylinder along opposite generatrices, or to a prism along the centre lines of opposite faces[3].

The splitting test has also been adopted for soils[4-6]; its application to asphalt, to the best of the authors' knowledge, is proposed for the first time. The recommendation of a prismatic specimen is based on considerations of field control requirements, the undisturbed specimens having to be prismatic in order to lend themselves both to horizontal and to vertical loading.

2. THE ELASTIC LIMIT STRESS IN THE SPLITTING TEST

The theory underlying the splitting test for concrete is based on a single property, namely tensile strength. This approach is impracticable for asphalt in view of its failure to agree with test results (see Section 5). In these circumstances, the proposed analysis is based on the characteristic strength properties of asphalt, namely the angle of internal friction, φ, and cohesion coefficient, C.

The elastic stress distribution along the diameter of a cylindrical specimen perpendicular to the loading stick is given (assuming the material to be weightless), according to Peltier[7], by eqs. (1a)–(1c) (see Figure 1).

$$\sigma_x = \frac{2pa}{\pi R}\left[\frac{R^2}{az}(\delta - \tfrac{1}{2}\sin 2\delta) - 1\right] \tag{1a}$$

$$\sigma_z = \frac{2pa}{\pi R}\left[\frac{R^2}{az}(\delta + \tfrac{1}{2}\sin 2\delta) + \frac{2R}{R+z} - 1\right] \tag{1b}$$

$$\tau_{xz} = 0 \tag{1c}$$

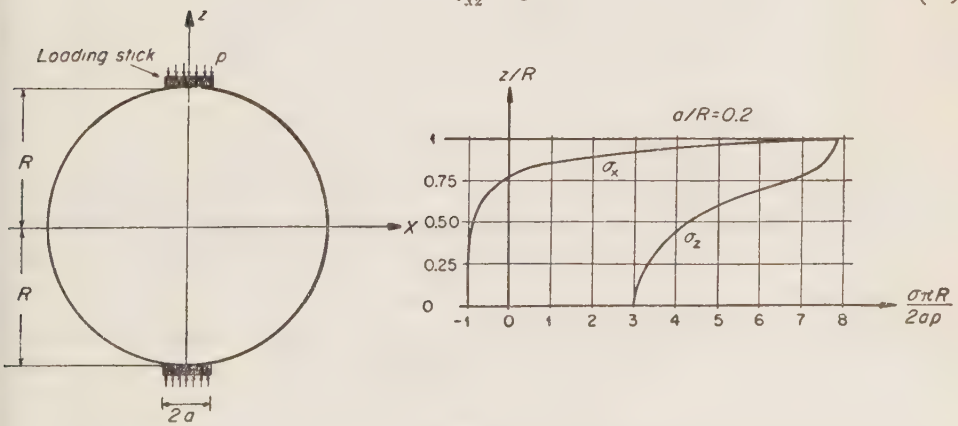

Figure 1
Elastic stress distribution in z-direction in splitting test

* For a literature survey on the splitting test for concrete, see Ref. (2).

where R is the specimen radius, $2a$ — the width of the loading sticks, p — the compressive stress uniformly distributed across each stick, σ_x and σ_z — axial stresses in the x- and z-directions respectively, τ_{xz} — shearing stress in the xz-directions, and the angle δ is defined as follows:

$$\tan\delta = \frac{az}{R(R-z)} \tag{1d}$$

In accordance with the above equations σ_z is compressive* and σ_x compressive at the edges of the specimen and tensile within it.

Assuming that the strength of the asphalt obeys Coulomb's law, namely that

$$S = C + \sigma_n \tan\varphi \tag{2}$$

where S is the shearing strength, C — the cohesion coefficient, φ — the angle of internal friction and σ_n—the stress normal to the plane of failure, then the following condition has to be satisfied at every point of the plane of failure:

$$\frac{(\sigma_1-\sigma_3)_f}{2} = \frac{C\cos\varphi}{1-\sin\varphi} + \frac{\sigma_3\sin\varphi}{1-\sin\varphi} \tag{3}$$

In this equation $(\sigma_1 - \sigma_3)_f$ denotes the difference of the principal stresses at failure (σ_1 being the major and σ_3 the minor principal stress). In practice, σ_x in eq. (1) represents σ_3 and σ_z represents σ_1, so that substitution of their difference in eq. (3), giving eq. (4), permits determination of the stress p_E corresponding to the limit load in the elastic range:**

$$\frac{p\times 2a}{\pi R}\left[\frac{R^2}{az}\left(\frac{\sin 2\delta}{2}+\frac{R}{R+z}\right)\right] = \frac{C\cos\varphi}{1-\sin\varphi} +$$

$$+\frac{p\times 2a}{\pi R}\left[\frac{R^2}{az}(\delta - \tfrac{1}{2}\sin 2\delta) - 1\right]\frac{\sin\varphi}{1-\sin\varphi} \tag{4}$$

Eq. (4) can also be rewritten in the following form, designating $\frac{C\pi R\cos\varphi}{pa}$ by F:

$$F = \left(\frac{1}{\tan\delta}+\frac{R}{a}\right)(\sin 2\delta - 2\delta\sin\varphi) + \frac{\frac{R}{a}\tan\delta + 1}{2\frac{R}{a}\tan\delta + 1}\times 2(1-\sin\varphi) + 2\sin\varphi \tag{5}$$

---

* In this paper, the plus sign denotes compression and the minus sign tension.

** It should be borne in mind that if this limit is exceeded, stress distribution will be affected and eq. (1) will no longer be valid for calculating the failure load.

The value δ_0, for which F is maximum, determines the coordinates of the initial point of the failure mechanism, namely for

$$\frac{dF}{d\delta} = 0 \tag{6}$$

we obtain

$$\frac{\sin 2\delta_0 - 2\delta_0 \sin\varphi}{2\sin^2\delta_0} + \frac{(1-\sin\varphi)R}{\left(2\frac{R}{a}\tan\delta_0 + 1\right)^2 a\cos^2\delta_0} = (\cos 2\delta_0 - \sin\varphi)\left(\frac{1}{\tan\delta_0} + \frac{R}{a}\right)$$

whose approximate solution* is

$$\tan\delta_0 = \tan(\pi/4 - \varphi/2) - \frac{a}{R} = \frac{1}{\sqrt{N_\varphi}} - \frac{a}{R} \tag{8}$$

where

$$N_\varphi = \frac{1}{\tan^2(\pi/4 - \varphi/2)} = \tan^2(\pi/4 + \varphi/2)$$

It can be shown that for $R/a = \infty$, the solution according to eq. (8) is quite exact.

Finally, substituting eq. (8) in eq. (5), we obtain

$$\frac{C\pi R\cos\varphi}{2p_E a} = \frac{\frac{R}{a}}{1 - \frac{a}{R}\sqrt{N_\varphi}}\left[\frac{\sqrt{N_\varphi} - \frac{a}{R}N_\varphi}{N_\varphi + \left(1 - \frac{a}{R}\sqrt{N_\varphi}\right)^2} - \sin\varphi \arctan\left(\frac{1}{\sqrt{N_\varphi}} - \frac{a}{R}\right)\right] +$$

$$+ \frac{(1-\sin\varphi)\frac{R}{a}}{2\frac{R}{a} - \sqrt{N_\varphi}} + \sin\varphi \tag{9}$$

It is of interest to consider the case $R/a = \infty$ (which is identical in practice with that of a semi-infinite elastic body, subjected to an infinite strip of load) as solved by Boussinesq. Substituting $R/a = \infty$ in eq. (9), we obtain

$$p_{E(R/a=\infty)} = \frac{C\pi\cos\varphi}{\cos\varphi - (\frac{\pi}{2} - \varphi)\sin\varphi} \tag{10}$$

* For example, for $R/a = 5$ and $\varphi = 30°$, the exact solution of δ_0 by eq. (7) gives 23°48′, while approximation according to eq. (8) gives 20°42′, the error involved in this approximation being (3.94–3.90)/3.90 = 1% for F and (3.44–3.27)/3.27 = 5% for z_0 (the coordinate of the point of failure).

A similar expression can obviously be arrived at by substituting the difference $(\sigma_z - \sigma_x)$ given in Boussinesq's formulae[8] in eq. (3) and proceeding as described above.

The next step is to see to what extent the above analysis is applicable to the prismatic specimens on which the proposed method is based. For $2a = 0$, solutions exist for:

(a) A prism of square cross-section (solution by means of the relaxation method[3]).
(b) A prism with an infinite rectangular horizontal cross-section[9]*.

Comparison of these solutions with one for a cylinder with $2a = 0$ leads to the conclusion that stress magnitudes and distributions are almost identical in all three cases.

For example, the respective stress for each section, at the mid-point of the axis joining the two points of application of the load, is given by

$$\sigma = \frac{k}{2} \frac{P}{R} \tag{11}$$

where P is the load per unit length, R — the radius or half-height of the specimen, and k a constant factor given in the following table:

k for different sections

Stress	Section		
	Infinite rectangular	Square	Circular
σ_x	− 0.484	− 0.642	− 0.636
σ_z	+ 1.824	+ 1.987	+ 1.908
$\sigma_z - \sigma_x$	+ 2.308	+ 2.629	+ 2.544

The numerical values in the table show that the elastic solution for the circular section is very close to the average of the square and the infinite–rectangular. Hence the conclusions arrived at above are also valid for the prismatic specimen. These conclusions are:

* This solution is based on the superposition of two identical simply-supported beams of infinite span, each subjected to the same single force at midspan acting in opposite directions, and is obtained by means of integration of series.

(a) The relative coordinates of the initial point of failure are independent of R/a, since by eq. (8), we have

$$\frac{a}{R-z} = \frac{1}{\sqrt{N_\varphi}} = \text{const.}$$

(b) The elastic limit stress increases with R/a [eq. (9)] tending to an asymptotic value for $R/a = \infty$ (eq. 10).

3. THE FAILURE STRESS IN THE SPLITTING TEST

The elastic limit stress p_E is not identical with the failure stress p_f. The former represents the initial point of the development of the failure mechanism and the latter — its end-point.

From conclusion (a) in the preceding section, it follows that the failure mechanism in its early stages is the same for prismatic specimens, irrespective of the h/a ratio (h being the half-height of the specimen); if the initial point coincides with the centre of the specimen, the possible mechanism is that of unconfined compression[10].

From conclusion (b), it follows that the failure stress increases with the h/a ratio and tends to an asymptotic value for $h/a = \infty$. This asymptotic value is in practice the failure stress according to Prandtl's theory[8]. Hence the failure mechanism in the splitting test has to correspond to either alternative according to the h/a range in question. Such a mechanism is described in Figure 2 (also giving the actual failure patterns obtained on asphalt specimens); for $\theta = 0$ it corresponds to the unconfined compression alternative, and for $\theta = \pi/2$ — to Prandtl's theory. The area bounded by points 1, 2, 3, 4, 5 comprises the zone of Prandtl's mechanism, lines 5–6 and 2–6 being assumed as circular in their upper part and straight in the lower part,* forming an angle of $(\pi/4 - \varphi/2)$ with the vertical axis of symmetry, which is the locus of the principal stresses. The transition point between the two parts is determined by the consideration that for $\theta = \pi/2$, $h/a = \infty$. This hypothesis is comparable to the failure mechanism proposed, on the basis of exact analysis, for a material with a curvilinear strength diagram[11] (see Figure 3).

The geometrical relationships for the proposed failure mechanism are

$$r_\theta = r_0 e^{\theta \tan\varphi};\quad x = r_0 \sin(\pi/4 + \varphi/2);\quad a = r_0 \cos(\pi/4 + \varphi/2). \tag{12}$$

$$h/a = \frac{(1 + e^{\theta \tan\varphi}) \sin\dfrac{\theta}{2}}{\sin(\pi/4 - \theta/2)\sin(\pi/4 - \varphi/2)}\left[\cos\varphi/2 + \sin\varphi/2\sqrt{N_\varphi}\right] + \sqrt{N_\varphi} \tag{13}$$

* The combination of circular arc and straight line was assumed for simplicity.

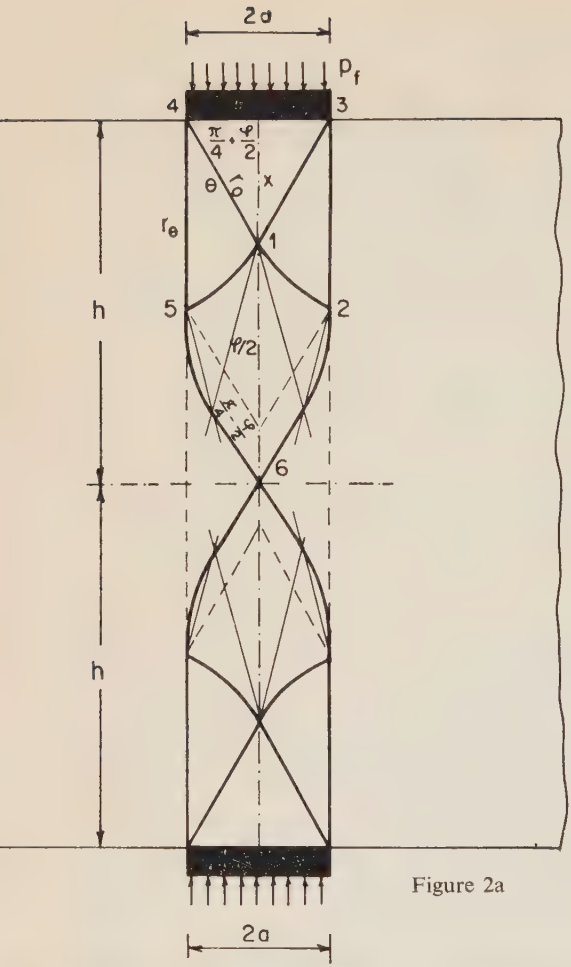

Figure 2a

Figure 2a
Theoretical failure mechanism in splitting te

Figure 2b
Failure patterns in asphalt specimens ($2a = 1$
(1) $2h = 6$cm (2) $2h = 12$c

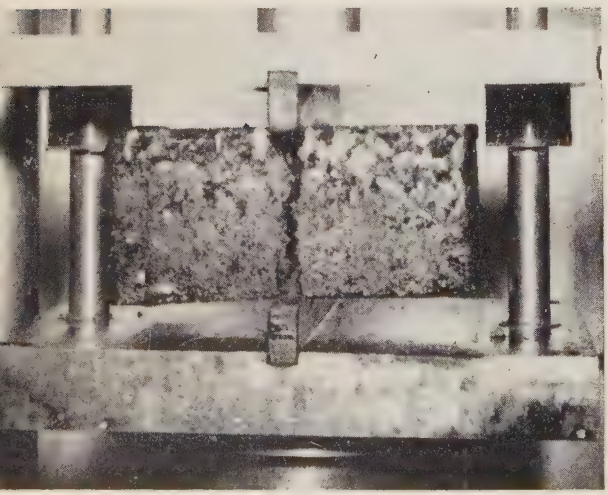

Figure 2b(1)

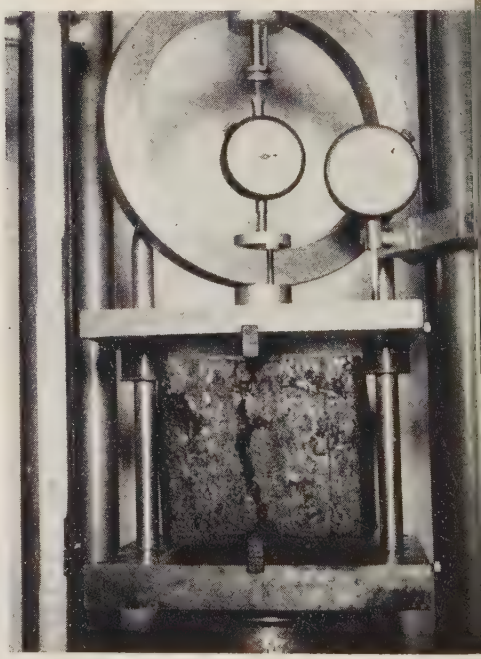

Figure 2b(2)

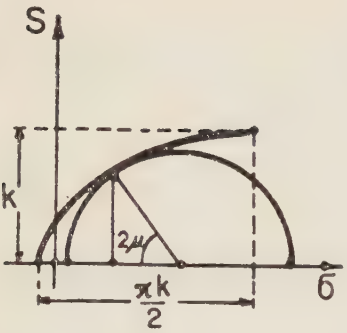

(a)

Figure 3(a)
Critical curve of shear envelope—curvilinear strength diagram (Ref. 11)

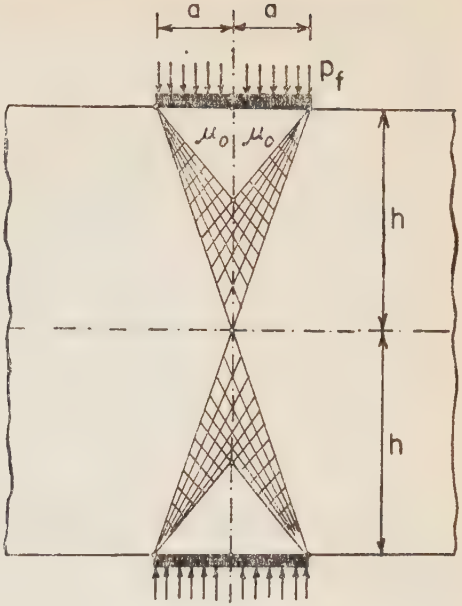

(b)

Figure 3(b)
Failure mechanism for shear envelope in (a)

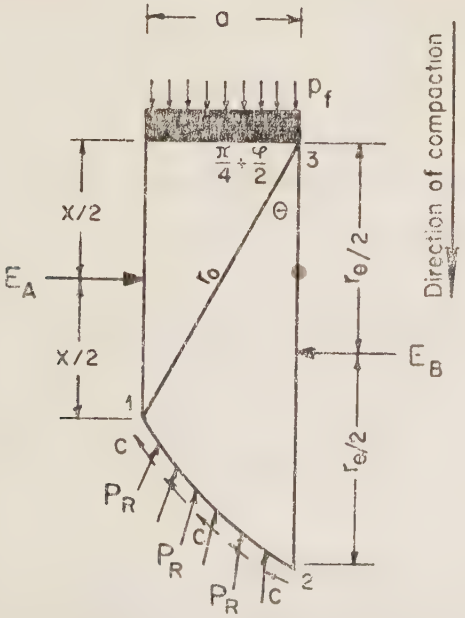

Figure 4
Forces acting on segment of failure mechanism

The failure stress p_f can be determined by substituting the forces acting on a segment of the proposed mechanism (see Figure 4). The sum of moments with respect to point 3 is

$$\frac{E_A}{2}x + \frac{p_f a^2}{2} = \frac{E_B r_\theta^2}{2} + \int_0^\theta C r_0 e^{2\theta \tan\varphi}\, d\theta \tag{14}$$

where

$$E_A = \frac{p_f}{N_\phi} - \frac{2C}{\sqrt{N_\phi}} \tag{15}$$

and

$$E_B = r_\theta C \cos\varphi \tag{16}*$$

Solving the integral in eq. (14) and substituting the appropriate values from eq. (12), (15) and (16) we have:

$$p_f = C \cot\varphi \left[e^{2\theta \tan\varphi} N_\varphi - 1\right] \tag{17}$$

Eqs. (13) and (17) give the relationship between p_f and h/a with the angle θ as parameter. It can be seen that:

(a) For $\theta = 0$, by eq. (13) $h/a = \sqrt{N_\varphi}$ and p_f, according to eq. (17), is the unconfined compression.

(b) For $\theta = \pi/2$, $h/a = \infty$ and p_f is the Prandtl compression.

4. THE EFFECT OF THE ANISOTROPIC COHESION ON THE FAILURE STRESS

The strength of the asphalt being anisotropic, the effect of this anisotropy on the failure stress in the splitting test should be studied. The strength diagram for asphalt is[12]

$$S = C_{perp} + (C_{par} - C_{perp})\sin^2\alpha_0 + (\sigma_{par} - \sigma_{perp})\cos^2\alpha_0 \tan\varphi \tag{18}$$

---

* The force E_B can only be determined provided σ_3, acting in the plane of failure 5–6 or 2–4, is known. Since this plane of failure does not form an angle of $(\pi/4–\varphi/2)$ with the horizontal boundary line (for which it is known that σ_3 is normal and zero), it must be assumed that the zone between the boundary and the plane forming an angle of $(\pi/4—\varphi/2)$ with 5–6 or 2–4 is stress-free; hence σ_3 for the above plane of failure is zero.

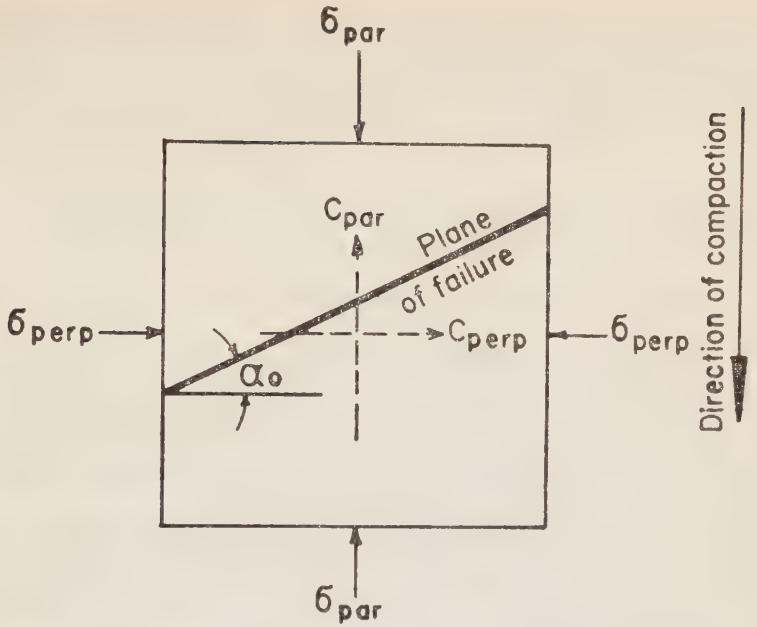

Figure 5
Scheme of principal stresses and cohesion relative to direction of compaction

where (see Figure 5)

C_{perp} = cohesion coefficient perpendicular to direction of compaction

C_{par} = cohesion coefficient parallel to direction of compaction

φ = angle of internal friction (constant for each direction)

σ_{par} = major principal stress, parallel to direction of compaction

σ_{perp} = minor principal stress, perpendicular to direction of compaction

α_0 = angle of inclination of plane of failure with respect to minor principal stress, given by

$$\tan\alpha_0 = \sqrt{\frac{C_{perp} + \sigma_{perp}\tan\varphi + (\sigma_{par} - \sigma_{perp})\tan\varphi}{C_{par} + \sigma_{perp}\tan\varphi}} \tag{19}$$

The strength diagram according to eq. (18) cuts the Mohr circles, while the tangent is given with sufficient accuracy by[12]

$$S' = C_m + (\sigma_1 - \sigma_3)\cos^2(\pi/4 + \varphi/2)\tan\varphi \tag{20}$$

where C_m is the apparent cohesion related to C_{perp}, C_{par} and φ and the angle between the major (σ_1) or minor (σ_3) principal stress and the direction of compaction. For the case where σ_{par} is the major stress we have $C = C_m$, and for that of the minor stress, $C_m = C/m$; for intermediate cases the following interpolation can be used

$$C_m = C + \left(\frac{C}{m} - C\right)\sin^2\beta \tag{21}$$

where β is the angle between the major principal stress and the direction of compaction.

In the case of anisotropic cohesion, the failure stress will be determined on the assumption of a strength diagram according to eq. (20). The principle underlying this assumption is based on the common soil engineering practice (known as the "$\varphi = 0$ analysis"[13]; see also Appendix) of approximating the actual strength diagram and failure mechanism by their apparent counterparts.

The apparent mechanism corresponding to the apparent strength diagram [eq. (20)] is one in which the angle between the failure lines and the principal stresses is $\pi/4 + \varphi/2$. It is similar to that described in Figures 2 and 4, except that the corresponding forces in this case are

$$E_A = \left[\frac{p_{par}}{N_\varphi} - \frac{2C}{\sqrt{N_\varphi}}\right] x \tag{22}$$

$$E_B = \left[C + \left(\frac{C}{m} - C\right)\sin^2\theta\right] r_\theta \cos\varphi \tag{23}$$

From the sum of moments with respect to point 3 we have

$$\frac{E_A x}{2} + \frac{p_{par}\, a^2}{2} = \frac{E_B r_\theta^2}{2} + \int_0^\theta [C + (C/m - C)\sin^2\theta] r_0^2\, e^{2\theta \tan\varphi}\, d\theta \tag{24}$$

Solving the integral in eq. (24) and substituting the appropriate values from eqs. (12), (22) and (23), we obtain

$$\frac{p_{par}}{C} = [e^{2\theta\tan\varphi} N_\varphi - 1]\cot\varphi \left[1 + \frac{(1/m-1)}{2}(1+\sin\varphi)\sin^2\theta\right] +$$

$$+ \frac{(1/m-1)}{2\tan\varphi}(1+\sin\varphi)\cos\theta(e^{2\theta\tan\varphi}\cos\theta - 2e^{2\theta\tan\varphi}\sin\theta - \cos\theta) \tag{25}$$

Eqs. (25) and (13) give the relationship between p_{par} and h/a with the angle θ as parameter (see Figure 6). For $\theta = 0$, eq. (25) is identical with eq. (17) which is its counterpart for an isotropic material, while for $\theta = \pi/2$, eq. (25) is equivalent to eq. (17) multiplied by $\frac{1}{2}[1 - \sin\varphi + (1 + \sin\varphi)/m]$ which is actually the anisotropy factor in compression according to Prandtl*.

Eq. (25) permits calculation of the ratio p_{par}/p_{perp}, given graphically in Figure 7 for $m = 3$. The figure shows that this ratio is smaller than m.

5. EXPERIMENTAL

On the strength of the above, a number of theoretical relationships can be derived and verified in laboratory experiments These are:

(a) The relationship between the respective failure stresses under parallel loading ($p_{par}^{(6)}$) and the unconfined compressive stress (also parallel, σ_u), for $h/a = 6$; results given in Figure 8 for $m = 1$ and 3 respectively.

(b) The relationship between the respective failure stresses under parallel loading for $h/a = 6$ nd $h/a = 12$ ($p_{par}^{(6)}$ and $p_{par}^{(12)}$); results also given in Figure 8 for $m = 1$ and 3 respectively.

(c) The relationship between the respective failure stresses under parallel and perpendicular loading for $h/a = 12$ ($p_{par}^{(12)}$ and $p_{perp}^{(12)}$); results given in Figure 9.

Specimens were prepared from crushed limestone (for grading see following table) bitumen (6% by weight), subjected to static compaction at 140°C to give different densities and tested after half an hour's soaking in hot water (60°C).

Grading of aggregates

A.S.T.M. sieve	3/4″	1/2″	3/8″	4#	10#	40#	80#	200#
% passing	100	80	68	52	38	17	11	6.5

Tests were carried out, at a steady rate of loading of 2 inch/min, as follows:

(a) Splitting test, using a 6 cm specimen and 1cm loading stick ($h/a = 6$), parallel loading ($p_{par}^{(6)}$).

* It is interesting to note that this anisotropy factor is identical with the one obtained when calculating the bearing capacity according to McLeod [12].

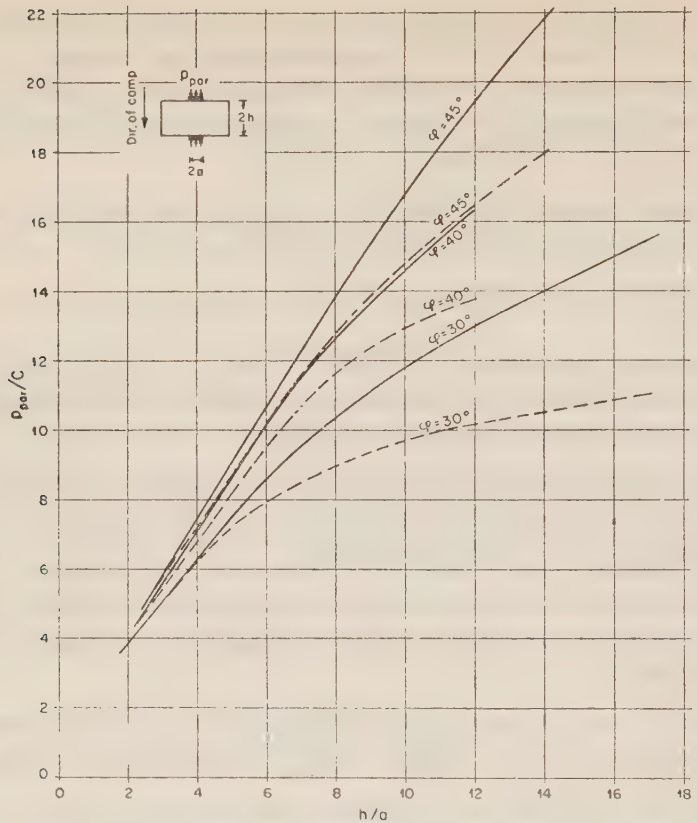

Figure 6
Failure stress/cohesion ratio vs. h/a (parallel loading) for $m = 1$ (solid line) and $m = 3$ (dashed line)

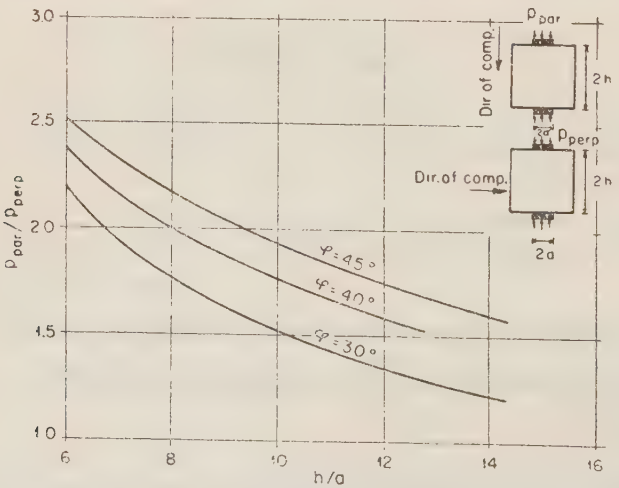

Figure 7
Failure stress ratio (parallel and perpendicular loading resp.) vs. h/a for $m = 3$

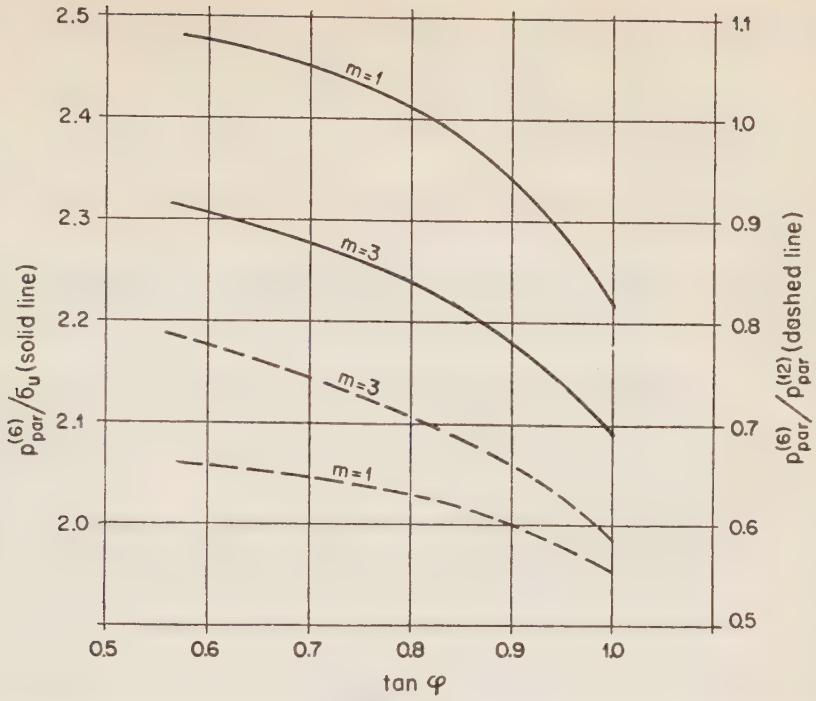

Figure 8

(a) Failure stress/unconfined compressive stress ratio vs. angle of internal friction for $h/a = 6$ (solid line) (parallel loading, $m=1$ and 3 resp.)

(b) Failure stress ratio ($h/a = 6$ and 12 resp.) vs. angle of internal friction (dashed line) (parallel loading, $m = 1$ and 3 resp.)

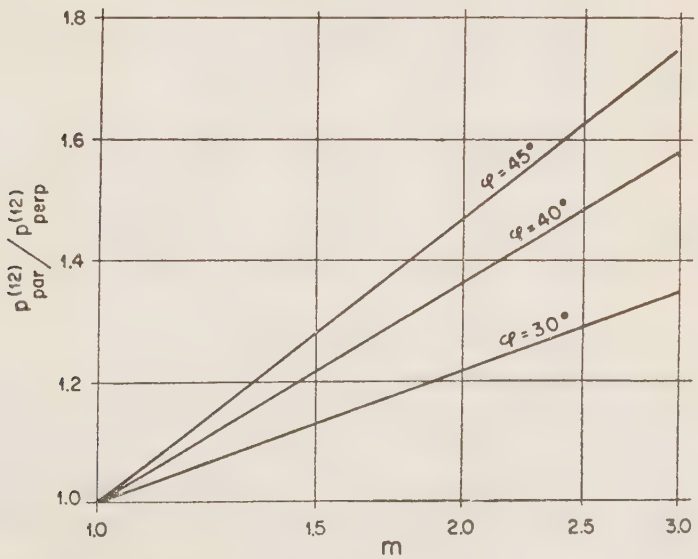

Figure 9

Failure stress ratio (parallel and perpendicular loading resp.) vs. apparent anisotropic cohesion, for $h/a = 12$

(b) Splitting test, using a 12cm specimen and the same loading stick as before ($h/a = 12$), lo ding perpendicular and parallel ($p_{perp}^{(12)}$ and $p_{par}^{(6)}$).

(c) Unconfined compression test, using a specimen 4″ in diameter and 6″ high, parallel loading (σ_u).

(d) Compression test, using a 12cm cube, perpendicular and parallel loading (σ_{perp}, σ_{par}).

Results are summarised in Figures 10, 11, and 12, giving failure stress against density. The ratios calculated as described at the beginning of this section are given in Figure 13.

Comparison of experimental and theoretical data (Figures 8 and 9) showed satisfactory agreement. Values of φ used for comparison should be above 40°. (It should also be borne in mind that the ratio $m' = \sigma_{par}/\sigma_{perp}$ is equivalent to m in order of magnitude only).

Ratios are summarised in the following table, showing that except for the low density of 2220 kg/m³ the deviation is of a reasonable order of magnitude, its maximum being 20% for the $p_{par}^{(12)}/p_{perp}^{(12)}$ ratio and the 2240 kg/m³ density. (For the 2220 kg/m³ density the maximum deviation is 27%, for the same ratio).

Ratio	Density (kg/m³)											
	2220			2240			2260			2280		
	Lab.	Theor. $\varphi=40°$	Theor. $\varphi=45°$	Lab.	Theor. $\varphi=40°$	Theor. $\varphi=45°$	Lab.	Theor. $\varphi=40°$	Theor. $\varphi=45°$	Lab.	Theor. $\varphi=40°$	Theor. $\varphi=45°$
1. $p_{par}^{(6)}/\sigma_u$	2.76	2.34	2.18	2.48	2.32	2.17	2.26	2.31	2.15	2.05	2.34	2.18
2. m'	1.70			1.86			1.92			1.65		
3. $p_{par}^{(12)}/p_{perp}^{(12)}$	1.76	1.29	1.38	1.65	1.33	1.42	1.54	1.34	1.44	1.44	1.24	1.32
4. $p_{par}^{(6)}/p_{par}^{(12)}$	0.60	0.64	0.58	0.60	0.65	0.59	0.61	0.66	0.60	0.64	0.64	0.58

6. CONCLUSIONS

The theory of the failure mechanism presented in this paper is especially useful for analysing results obtained in splitting tests of field specimens of varying thickness. In addition, determination of the bearing capacity of the asphalt involves that of the m ratio, which is a function of the anisotropy of cohesion in field specimens; but since only the p_{par}/p_{perp} ratio lends itself to laboratory determination the relationship between m and the latter must also be ascertained.

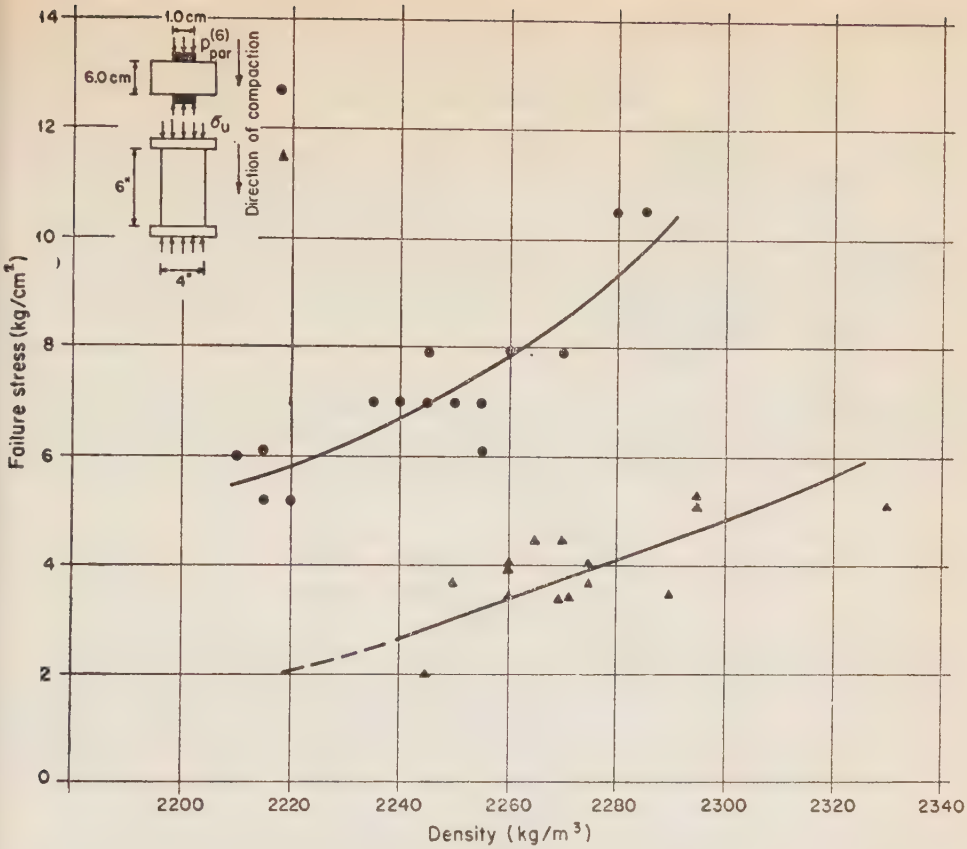

Figure 10
Failure stress vs. density in splitting test ($h/a=6$) and unconfined compression test, parallel loading

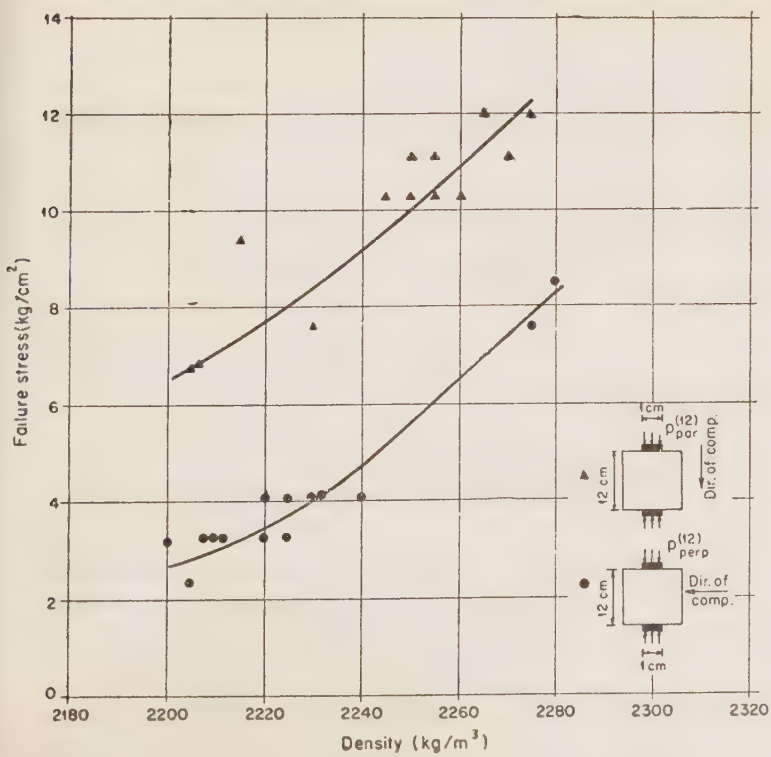

Figure 11
Failure stress vs. density ($h/a = 12$), parallel and perpendicular loading

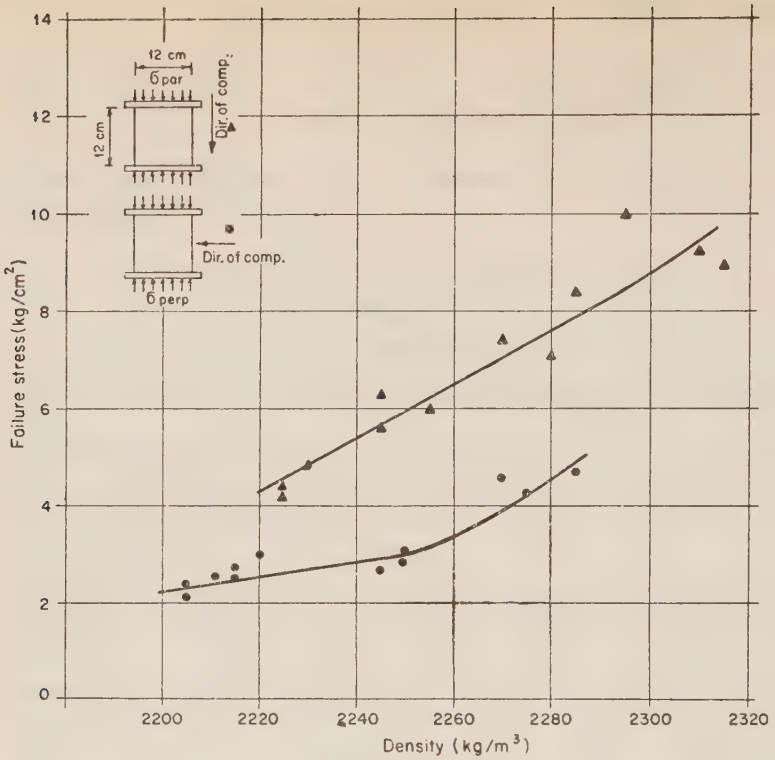

Figure 12
Failure stress vs. density in compression test, parallel and perpendicular loading

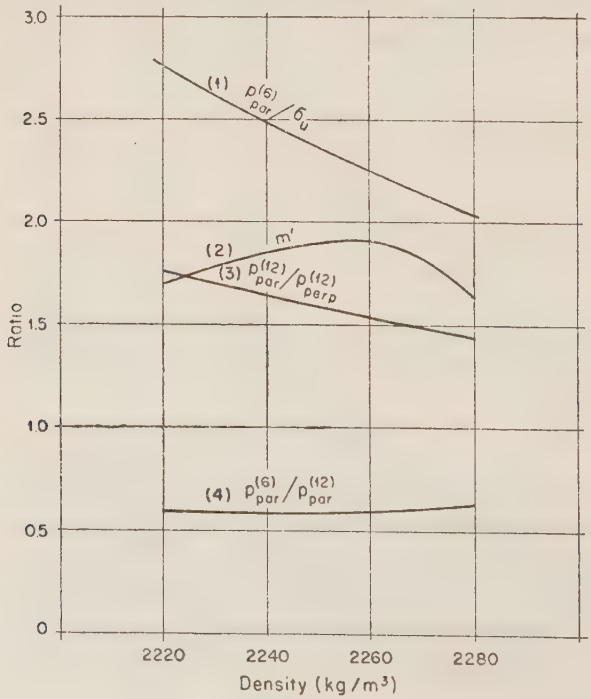

Figure 13
Ratios obtained in splitting and compression tests vs. density

In view of the satisfactory agreement between theoretical and experimental results, it can be concluded that:

(a) The theoretical relationship between p_{par} and h/a (Figure 6) can be used for calculating the equivalent failure stress for a specimen of standard h/a (recommended value — 6) on the basis of failure stresses determined on specimens of different h/a.

(b) The theoretical relationship between the ratio p_{par}/p_{perp} and h/a (Figure 7) can be used for calculating m on the basis of splitting tests under perpendicular and parallel loading.

APPENDIX

The failure mechanism for $h/a = \infty$ in the case of anisotropic cohesion and zero internal friction angle is described in Figure 14a.

The forces involved are (see Figure 14b):

$$\left.\begin{aligned} C_\alpha &= C_{perp} + (C_{perp} - C_{par})\sin^2\alpha \\ E_A &= \left(p - 2\sqrt{C_{par}\,C_{perp}}\right)x \\ E_p &= 2\sqrt{C_{par}\,C_{perp}}\;x \end{aligned}\right\} \qquad \text{(a)*}$$

The geometrical relationships in this mechanism are

$$\left.\begin{aligned} &x = a\tan\alpha_0; \quad b = a/\cos\alpha_0; \quad d = 2a/\tan 2\alpha_0 \\ &r = a/\sin\alpha_0; \quad \tan\alpha_0 = \sqrt{C_{perp}/C_{par}} \end{aligned}\right\} \qquad \text{(b)**}$$

The sum of moments with respect to point 0 gives

$$E_a\left(\frac{x}{2} + d\right) + p\,\frac{a^2}{2} - E_p\left(\frac{x}{2} + d\right) + 2\int_0^{\alpha_0} r^2 C_\alpha d\alpha = 0 \qquad \text{(c)}$$

* Obtained by substituting $\varphi = 0$ in eq. (18). The radius of Mohr's circle described by varying α is $\sqrt{C_{perp}\,C_{par}}$ (See Figure 14c).

** Obtained by substituting $\varphi = 0$ in eq. (19).

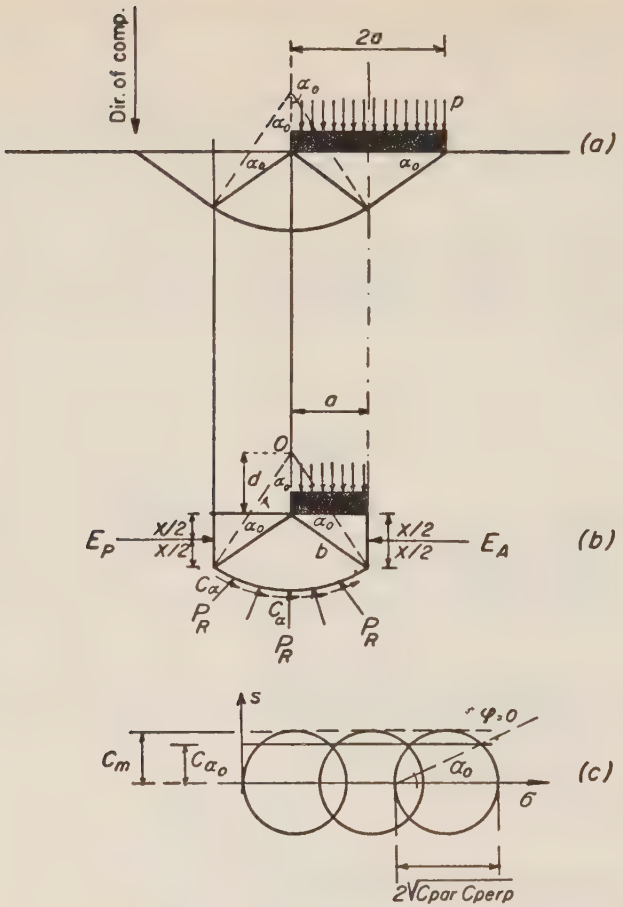

Figure 14

(a) Failure mechanism in semi-infinite specimen
(b) Forces in failure mechanism (a)
(c) Anisotropic envelope for $\varphi = 0$

Solving the integral in eq. (c) and substituting the appropriate values from (a) and (b) we have

$$p = \sqrt{C_{perp}/C_{par}} \left[\frac{4(2C_{perp} - C_{par})C_{par} - 2(C_{perp} - C_{par})C_{perp} + 2(C_{perp} + C_{par})^2}{(3C_{perp} - C_{par})C_{par}} \right] \quad \text{(d)}$$

$$\tan\alpha_0 = \alpha_0 = \sqrt{\frac{C_{perp}}{C_{par}}} \qquad \text{for } C_{par}/C_{perp} \to \infty \quad \text{(e)}$$

hence the bearing capacity is

$$p = \frac{14\,C_{par}\,C_{perp} - 2C^2_{par}}{(3C_{perp} - C_{par})\,C_{par}} \sqrt{C_{par}\,C_{perp}}$$

and for $\frac{C_{par}}{C_{perp}} = \infty$, $\qquad p = 4.7\sqrt{C_{par}\,C_{perp}}$ (f)

The apparent strength diagram of the asphalt* is given by

$$C_m = \sqrt{C_{par}\,C_{perp}} = \text{const.} \tag{g}$$

$$\varphi = 0$$

$$\alpha_0 = \pi/4$$

hence the bearing capacity calculated from it is

$$p = 5.12\sqrt{C_{par}\,C_{perp}}$$

Comparing (h) with (f), it can be seen that the error involved in substituting the apparent strength line is only 10%, and this only for the extreme case of $C_{par}/C_{perp} = \infty$. For smaller values the error will decrease, hence the use of this simplified method is justified in practice.

REFERENCES

1. The Asphalt Institute, 1957, Mix design methods for hot-mix asphalt paving, Manual Series No. 2
2. Jaegermann, C. H., 1960, A comparative and experimental analysis of accepted and proposed tests for measuring the tensile strength of concrete, *M.Sc. Thesis*, Technion–Institute of Technology, Haifa (In Hebrew).
3. Rosenhaupt, S., van Riel, A. C. and Wijler, L., 1957, A new indirect tensile test for concrete—theoretical analysis and preliminary experiments, *Bull. Res. Counc. of Israel*, **6C**, (1).
4. Kyvellos, M. G., 1959, Etude de la courbe intrinséque des sols compactes et non saturés, *Annales de l'Institut Technique du Bâtiment et des Travaux Publics*, No. 101.
5. Alpan, I., 1959, A study of the principle of effective stress in partly saturated soils, *Ph. D. Thesis*, London University, Appendix 7.
6. Kirkham, D., De Boodt, M. and De Leenheer, L., 1958, Modulus of rupture determination on cylindrical soil core samples, *International Symposium on Soil Structure*, Ghent, May 28–31.
7. Peltier, R., 1954, Theoretical investigation of the Brazilian test, International Association of Testing and Research Laboratories, *Bull. No.* 19, *Paris*, 26–29.
8. Terzaghi, K., 1948, *Theoretical Soil Mechanics*, Wiley, New York. pp. 376–377, 127–128.
9. Timoshenko, S. and Goodier, J. N., 1951, *Theory of Elasticity*, McGraw-Hill, New York, pp. 102–106.

* The tangent to Mohr's circles in Figure 14c (dashed line), the actual strength diagram being the line cutting the circles (solid line).

10. VAN ITERSON, F. K. TH., 1947, *Plasticity in Engineering*, Blackie, London, pp. 57–58.

11. SOKOLOVSKI, V. V., 1960, *Statics of soil media*, Butterworths Scientific Publications, London, pp. 225–232.

12. SHKLARSKY E. AND LIVNEH M., 1961, The anisotropic strength of asphaltic paving mixtures, *Bull. Res. Counc. of Israel*, **9C**, (4).

13. SKEMPTON, A. W., 1948, The $\varphi = 0$ analysis of stability and its theoretical basis, *Proc. 2nd Int. Conf. Soil Mech.*, **1**, 72–78.

A SYMPOSIUM ON BASIC PROBLEMS OF SPACE TRAVEL

Monday afternoon, 3.4.61 Chairman: D. ABIR

Interplanetary matter and planetary atmospheres

J. NEUMANN, *Department of Meteorology, The Hebrew University of Jerusalem*

This paper reviews progress since the launching date of the first artificial Earth satellite.

Interplanetary matter. The major discovery is the existence of the Van Allen radiation belts around the Earth extending outward to several Earth radii. There are some indications that, at least, one of the other planets (viz. Jupiter) possesses similar belts.

The atmospheres of both the Sun and Earth (and, presumably, those of other planets as well) extend to greater distances than assumed heretofore. The Earth, e.g., is apparently within the Sun's outer corona. Influx of matter from solar storms causes pronounced variations in upper atmospheric densities. Data have been gathered on meteoritic particles about the Earth and on the rate of accretion to Earth of such matter. Clouds of ionized particles, carrying a magnetic field, are likely to be encountered in interplanetary space.

Planetary atmospheres. A considerable body of data has been obtained on the outer reaches of the Earth's atmosphere, while special satellites have taken photographs showing that cloud systems in the lower terrestrial atmosphere have a spiral structure. The latter give rise to new ideas on circulation conditions within these storms. Considerable work has been done on the subject of the tenuous lunar atmosphere.

Concerning the other planets, the most significant discovery is the definite identification of (small amounts of) water vapour above the visible surface of Venus. The discovery was made from a balloon, without recourse to the more expensive rockets or satellites. Earlier ideas, suggesting a thick atmosphere over Venus, are giving way to hypotheses supporting a relatively thin atmosphere. Because of the high planetary albedo of Venus, its average atmospheric temperature is probably lower than that for Earth. Fundamental astronomic data in respect to Venus are still uncertain, but if it is true that the rotation period of the planet is something like three (terrestrial) weeks, then, it is probable that meridional circulations dominate the atmospheric motion.

Little additional knowledge has been gained in respect to the other planets, but indications of a low-level plant life on Mars have strengthened.

Reentry of space vehicle into planetary atmosphere

J. ROM (RABINOWICZ), *Department of Aeronautical Engineering, Technion–Israel Institute of Technology, Haifa*

The flight conditions of a space vehicle reentering a planetary atmosphere at extremely high speeds (18,000–33,000 ft/sec) have to be known for the design of a recoverable manned or instrumented space vehicle. The extremely high energy that is dissipated in the deceleration of the vehicle is manifested in the heating of the vehicle and in thermodynamical changes in the state of the air. Some of these problems and suggested solutions will be discussed.

Terrestial radiation belts

H. KASHA, *Physics Department, Technion–Israel Institute of Technology, Haifa*

An account is given of the discovery of the Van Allen radiation belts and of the evidence obtained in flight of satellites and rockets, on the form of the belts and the nature of the particles trapped in them. The implications of the discovery on manned space flight is discussed.

Basic problems of space travel

A. YARON, *Scientific Department, Ministry of Defense*

a. Theorem of conservation of momentum; rockets as means for obtaining high flight velocity; stage rockets and staging techniques.

b. Rocket efficiency parameters; specific impulse; propellant characteristics; review of the state of the art.

c. Design problems; search after construction materials for space travel.

d. Problems of human space travel; weightlessness, resistance to acceleration.

• Volume 9C, Number 4, May 1961

מוסד ויצמן לפרסומים במדעי הטבע ובטכנולוגיה בישראל • ירושלים

BULLETIN OF THE RESEARCH COUNICL OF ISRAEL

Section C
TECHNOLOGY

Bull. Res. Counc. of Israel. C. Techn.

Incorporating the Scientific Publications of the Technion — Israel Institute of Technology, Haifa

INDEX

TO

VOLUME 9C

The Weizmann Science Press of Israel • Jerusalem

NOTICE TO CONTRIBUTORS

Contributors to the *Bulletin of the Research Council of Israel* should conform to the following recommendations of the editors of this journal in preparing manuscripts for the press.

Contributions must be original and should not have been published previously. When a paper has been accepted for publication, the author(s) may not publish it elsewhere unless permission is received from the Editor of this journal.

Papers may be submitted in English and in French.

MANUSCRIPT

General

Papers should be written as concisely as possible. MSS should be typewritten on one side only and double-spaced, with side margins not less than 2.5 cm wide. Pages, including those containing illustrations, references or tables, should be numbered.

The Editor reserves the right to return a MS to the author for retyping or any alterations. Authors should retain copies of their MS.

Spelling

Spelling should be based on the Oxford Dictionary and should be consistent throughout the paper. Geographic and proper names in particular should be checked for approved forms of spelling or transliteration.

Indications

Greek letters should be indicated in a legend preceding the MS, as well as by a pencil note in the margin on first appearance in the text.

When there is any room for confusion of symbols, they should be carefully differentiated, e.g. the letter "1" and the figure "1"; "O" and "0".

Abbreviations

Titles of journals should be abbreviated according to the *World List of Scientific Periodicals*.

Abstract

Every paper must be accompanied by a brief but comprehensive abstract. Although the length of the abstract is left to the discretion of the author, 3% of the total length of the paper is suggested.

References

In Sections A and C, and in Letters to the Editor in all Sections, references are to be cited in the text by number, e.g. ... Taylor' ..., and are to be arranged in the order of appearance.

In Sections B, D, E, and G, the references are to be cited in the text by the author's name and date of publication in parentheses, e.g. ... (Taylor 1932)... If the author's name is already mentioned in the text, then the year only appears in the parentheses, e.g. ... found by Taylor (1932)... The references in these Sections are to be arranged in alphabetical order.

In Section F, references are to be cited in the text by number in square brackets, e.g. ... Taylor[3].., and are to be arranged in alphabetical order.

The following form should be used:

3. TAYLOR, G.I., 1932, *Proc. roy. Soc.*, A138, 41.

Book references should be prepared according to the following form:

4. JACKSON, F., 1930, *Thermodynamics*, 4th ed., Wiley, New York.

TYPOGRAPHY

In all matters of typography the form adopted in this issue should be followed. Particular attention should be given to position of symbols, headings, etc. and type specification.

ILLUSTRATIONS

Illustrations should be sent in a state suitable for direct photographic reproduction. Line drawings should be drawn in large scale with India ink on white drawing paper, bristol board, tracing paper, blue linen, or blue-lined grahp paper. If the lettering cannot be drawn neatly by the author, he should indicate it in pencil for the guidance of the draftsman. Possible photographic reduction should be carefully considered when lettering and in other details.

Half-tone photographs should be on glossy contrast paper.

Illustrations should be mounted on separate sheets of paper on which the caption and figure number is typed. Each drawing and photograph should be identified on the back with the author's name and figure number.

The place in which the figure is to appear should be indicated on the margin of the MS.

PROOFS

Authors making revisions in proofs will be required to bear the costs thereof. Proofs should be returned to the Editor within 24 hours, otherwise no responsibility is assumed for the corrections of the author.

REPRINTS

Reprints may be ordered at the time the proof is returned. A table designating the cost of reprints may be obtained on request.

Orders in America should be addressed to the Weizmann Science Press, P.O.B. 801 Jerusalem or through booksellers, and in England and Europe to Wm. Dawson and Sons, Ltd. Cannon House, Macklin Street, London W.C. 2, directly or through booksellers. Annual subscription per section (four issues): IL. 6.000 ($6.00, £2.02). Single copy: IL. 1.500 $1.50. 12s.) — Manuscripts should be addressed: The Editor, The Weizmann Science Press of Israel, P.O.B. 801 Jerusalem, 33 King George Ave. Telephone 27844, 26345.

INDEX

TO VOLUME 9C

CONTENTS

AUTHOR INDEX

SUBJECT INDEX

T

U

V

W

יוצא לאור ע"י
מוסד ויצמן לפרסומים במדעי הטבע ובטכנולוגיה בישראל
המועצה המדעית לישראל - משרד החנוך והתרבות - האוניברסיטה העברית בירושלים
הטכניון — מכון טכנולוגי לישראל - מכון ויצמן למדע - מוסד ביאליק

Published by
THE WEIZMANN SCIENCE PRESS OF ISRAEL
Research Council of Israel, Ministry of Education and Culture
The Hebrew University of Jerusalem, Technion—Israel Institute of Technology
The Weizmann Institute of Science, Bialik Institute

Printed in Israel
JERUSALEM ACADEMIC PRESS LTD.
SET ON MONOTYPE

WSP/1000/8.61/88